J. Mech. Phys. Solids 171 (2023) 105163

Contents lists available at ScienceDirect

Journal of the Mechanics and Physics of Solids

journal homepage: www.elsevier.com/locate/jmps

Chiral nonreciprocal elasticity and mechanical activity

Mohamed Shaat, Harold S. Park *

Department of Mechanical Engineering, Boston University, Boston, MA 02215, USA

ARTICLE INFO

Keywords:
Asymmetric elasticity
Nonreciprocal elasticity
Chiral metamaterials
Mechanical activity
Static non-equilibrium

ABSTRACT

There has been significant recent interest in creating, modeling, and exploiting the novel functionality afforded by odd elastic solids, which are a specific class of active matter whose behavior cannot be described by a free energy function. As a result, the mechanical behavior of such solids can be described by a non-symmetric elasticity tensor which means they can be mechanically active, and thus do work on their surroundings through quasistatic deformation cycles without energetic gain or loss terms explicitly appearing in the solid's equation of state. However, previous incarnations of such solids have required the usage of active elements coupled with robotic machinery powered by independent external energy sources to operate. As such, it is unclear whether the non-symmetric elasticity of these solids can be developed using only passive elements that do not require the usage of energy sources, and furthermore how nonreciprocity in elastic media enables non-symmetric elasticity in elastic solids or mechanical activity. In this work, we propose the notion of *chiral, nonreciprocal elasticity*, which represents a generic route to enabling 2D, isotropic elastic solids exhibiting non-symmetric elasticity. Chiral, nonreciprocal elasticity describes elastic behaviors that result from coupling chirality with nonreciprocity—specifically, (1) the modulation of the elastic properties depending on the mode and direction of deformation and (2) the nonreciprocal coupling of different deformation fields, both of which enable the solid to exhibit a non-symmetric elasticity tensor. To motivate this, we introduce an isotropic 2D chiral metamaterial made of passive chiral elements that, by exploiting local geometric asymmetry, behaves in a chiral, nonreciprocal elastic fashion. We derive, based on the mechanics of a discrete model of this chiral element, the resulting continuum field equations and constitutive relationships that capture the chiral, nonreciprocal elastic behavior. Then, we establish a thermodynamic framework of energy balance and conservation of chiral, nonreciprocal elastic solids, based on which we demonstrate the ability of the proposed chiral metamaterial to act as a source of mechanical work when used in specific quasistatic deformation cycles, though no energy is dissipated by its passive elements. Finally, we demonstrate through numerical finite element simulations the practical implementation of the deformation cycles, while elucidating the specific conditions needed for the chiral metamaterial to exhibit linear, chiral nonreciprocal elastic behavior throughout the deformation cycle, and thus reveal mechanical activity.

1. Introduction

A passive, elastic solid operating under thermodynamic equilibrium interacts with its surroundings through reversible processes, and thus its deformations must be path-independent, which requires knowledge of only the initial and final equilibrium states (De-Groot and Mazur, 1962). Deviation from this passive behavior often requires an active solid that is capable of violating energy

* Corresponding author.
E-mail address: parkhs@bu.edu (H.S. Park).

https://doi.org/10.1016/j.jmps.2022.105163
Received 25 April 2022; Received in revised form 21 November 2022; Accepted 23 November 2022
Available online 2 December 2022

conservation either by irreversible interactions with its surrounding environment, or through the motion or activity of internal mechanisms and energy sources. Therefore, motivated by the activity of motile organisms that range from animal flocks to bacterial swarms (Kumar et al., 2014; Patteson et al., 2018; Bowick et al., 2022), there has been significant interest in designing and obtaining biomimetic active solid metamaterials, which can violate thermodynamic equilibrium, and thus do work on their surroundings. Specifically, understanding the activity of living active matter has led to the development of self-propelled colloids (Theurkauff et al., 2012; Palacci et al., 2013), active filaments and molecular motors (Schaller et al., 2010; Sumino et al., 2012; Sanchez et al., 2012), self-propelled polar disks and rods (Deseigne et al., 2010; Kudrolli et al., 2008) and robot swarms (Rubenstein et al., 2014; Fruchart et al., 2021). This has also led to various routes enabling active solid metamaterials to achieve thermodynamic non-equilibrium (Das et al., 2020; Shankar et al., 2020; Asadchy et al., 2020; Nassar et al., 2020b). Most of these routes involve the use of space–time modulators to break time reversal symmetry (Asadchy et al., 2020; Taravati and Caloz, 2017; Correas-Serrano et al., 2016; Hadad et al., 2015; Shaltout et al., 2015; Estep et al., 2014; Fang et al., 2012a,b; Trainiti et al., 2019; Huang and Zhou, 2019; Lu and Norris, 2020), dynamics to achieve activity and non-reciprocity (Trainiti et al., 2019; Huang and Zhou, 2019; Nash et al., 2015; Zhao et al., 2020), mechanisms of feedback/control to generate nonreciprocal linear or angular momentum (Rosa and Ruzzene, 2020; Sirota et al., 2020; Brandenbourger et al., 2019), or mechanisms of local sensing, actuation and control to create motion, generate work, and violate thermodynamic equilibrium (Chen et al., 2021b). These routes have led to the development of active robotic metamaterials (Brandenbourger et al., 2019), gyroscopic topological metamaterials (Nash et al., 2015), and metamaterials for realizing non-Hermitian (Li et al., 2019a; Scheibner et al., 2020; Ghatak et al., 2019; Gong et al., 2018; Li et al., 2019b; Kunst and Dwivedi, 2019; Yao et al., 2018) and nonreciprocal (Taravati and Caloz, 2017; Correas-Serrano et al., 2016; Hadad et al., 2015; Shaltout et al., 2015; Estep et al., 2014; Sounas et al., 2013; Jin and Argyropoulos, 2019; Coulais et al., 2017; He et al., 2018) physical systems.

There is also significant interest in developing continuum constitutive models that can describe the behavior of active material systems (Markovich et al., 2019; Sabrina et al., 2015; Scheibner et al., 2020; You et al., 2020; Tjhung et al., 2017). In active matter, the active interactions between the material blocks may drive the material system out of thermodynamic equilibrium. The averaging of these active interactions at the continuum level may result in force or torque dipoles that give rise to active stresses, which can be symmetric (Markovich et al., 2019; Voituriez et al., 2005), chiral (Markovich et al., 2019; Tjhung et al., 2017; Soni et al., 2015; Sabrina et al., 2015), or non-symmetric (Condiff and Dahler, 1964; Naganathan et al., 2014, 2016). These active stresses can produce spontaneous motion of the system particles, and thus can drive the system to break thermodynamic equilibrium. Recently, odd viscosity was introduced to describe the behavior of active, chiral fluids with asymmetric active stresses that can break parity and time-reversal symmetries (Banerjee et al., 2017) or can achieve odd (or Hall) viscous behaviors (Avron, 1998). In chiral fluids, torque dipoles that produce non-conservative angular momenta can be developed, which give rise to energy gain/loss (Banerjee et al., 2017; Shankar et al., 2020). In analogy, the concept of odd elasticity was recently introduced to describe the behavior of active solids as elastic continua with non-symmetric elasticity tensors (Scheibner et al., 2020), whose mechanical behavior cannot be described by a free energy function. As a result, odd elastic solids can be active through quasistatic deformations, as the non-symmetric elasticity tensor enables energy non-conservation, which, importantly, can be achieved without energy gain/loss terms explicitly appearing in the solid's equations of motion.

Odd elastic solids have been proposed theoretically based on active springs with nonreciprocal forces (Scheibner et al., 2020), and experimentally based on active elements of metabeams with piezoelectric patches (Chen et al., 2021b). Whereas these previously proposed odd elastic solids can exhibit asymmetric elasticity, and thus be mechanically active at zero-frequency, achieving asymmetric elasticity required the presence of external (independent) energy sources such as batteries (Scheibner et al., 2020), or electrical circuitry (Chen et al., 2021b) along with controllers to actuate and control the motion of the utilized active components such that they can develop nonreciprocal forces/torques. An important question thus arises, which we resolve here—given this need for active elements with external sources of energy and momentum to obtain asymmetric elasticity, and thus odd elastic active solids, can such solids be developed using only passive elements that do not require external sources of energy or momentum to operate? Furthermore, and of equal importance, whereas it was revealed that Parity symmetry is broken by non-symmetric elasticity (Scheibner et al., 2020; Chen et al., 2021b), which results in nonreciprocal behaviors that can drive activity in material systems (Fruchart et al., 2021; You et al., 2020), it is not clear how nonreciprocity in elastic media enables non-symmetric elasticity, or – in general – activity in elastic solids at zero-frequency.

Here, we propose the notion of *chiral, nonreciprocal elasticity* - a generic route to enabling 2D isotropic solids that behave linear elastically and exhibit a non-symmetric elastic response. Chiral, nonreciprocal elasticity describes elastic behaviors that result due to combining *nonreciprocity*, which causes the mechanical response and the elastic properties of the solid to differ depending on the direction of the applied loading (Shaat, 2020; Coulais et al., 2017), with *chirality*, where the structure of the solid cannot be superimposed on its mirror transformation through any translation or rotation (Lakes, 2001). Because chirality enables the *reciprocal* coupling of different deformation fields (e.g., dilation to rotation/twist and dilation to shear) that would otherwise require anisotropy to achieve (Fernandez-Corbaton et al., 2019; Wu et al., 2019; Liu and Hu, 2016), the addition of non-reciprocity in the chiral interactions enables chiral, nonreciprocal elastic solids to have non-symmetric elasticity tensors and be mechanically active—specifically, mechanical work can be developed by using chiral, nonreciprocal elastic solids through closed quasistatic deformation cycles, and thus such solids can act as sources of mechanical work. In addition to the asymmetric elasticity manifested in odd elasticity, chiral, nonreciprocal elasticity also provides a new route to making solids whose elastic response is non-symmetric without external sources of energy, circumventing the aforementioned limitations of the existing odd elastic, active metamaterials (Trainiti et al., 2019; Nash et al., 2015; Rosa and Ruzzene, 2020; Sirota et al., 2020; Brandenbourger et al., 2019; Chen et al., 2021b; Li et al., 2019a; Scheibner et al., 2020). We first introduce chirality within the context of 2D isotropic elasticity, and then introduce the

formalism of chiral, nonreciprocal elasticity. We then introduce a 2D isotropic chiral metamaterial made of passive chiral elements that is chiral, nonreciprocal elastic, and derive, based on the mechanics of a discrete model of the chiral element, the continuum field equations and constitutive relationships that capture the chiral, nonreciprocal elastic behavior of the chiral metamaterial. Next, we develop a thermodynamic framework of energy balance and energy conservation of chiral, nonreciprocal elastic solids, based on which we demonstrate the ability of the chiral metamaterial to violate static thermodynamic equilibrium by developing work through specific quasistatic deformation cycles though no energy is dissipated/consumed by its passive, chiral elements. Finally, we show through numerical finite element simulations, the practical implementation of the deformation cycles, while elucidating the specific conditions needed for the chiral metamaterial to exhibit linear, chiral nonreciprocal behavior throughout the deformation cycle, and thus reveal mechanical activity.

2. Chiral, nonreciprocal elasticity

Before introducing the specific notion of chiral, nonreciprocal elasticity, we first introduce and define chirality within the context of 2D linear elasticity. A tensor is chiral if it breaks the reflection–rotation symmetry such that its parity inversion is not equivalent to its rotation in the spatial space (Scheibner et al., 2020). In 3D, even-rank tensors, e.g., Cauchy elasticity tensors C_{ijkl}, obey the reflection–rotation symmetry, and thus they are always achiral (Scheibner et al., 2020; Lakes, 2001). However, in 2D, even-rank tensors can be chiral with broken reflection–rotation symmetry (Scheibner et al., 2020). Chiral solids are distinct from their achiral counterparts with their ability to exhibit coupling between different deformation modes, e.g., coupled dilation–rotation, coupled dilation–twist, and coupled dilation–shear (Liu et al., 2012; Frenzel et al., 2017, 2019; Nassar et al., 2020a; Fernandez-Corbaton et al., 2019; Wu et al., 2019; Liu and Hu, 2016). Whereas these coupled deformations can also be exhibited by anisotropic solids, here we demonstrate that the existence of such coupled deformations in 2D isotropic solids is possible only through chirality, while elucidating the chiral elasticity tensor of 2D isotropic, chiral solids. We then demonstrate the chiral, nonreciprocal elasticity tensor that enables mechanical activity of 2D isotropic solids.

2.1. Chiral elasticity tensor

Consider a 2D isotropic elastic solid whose motion can be described by the two in-plane displacements $u_i(\mathbf{x}) \rightarrow (u_x(\mathbf{x})$ and $u_y(\mathbf{x}))$, where $\mathbf{x}$ is the spatial position in the 2D domain of the elastic solid. The equations of motion of the solid can be written, as follows:

$$\tau_{ji,j} + f_i = \rho \ddot{u}_i \tag{1}$$

where $\blacksquare_{,\alpha} = \partial\blacksquare/\partial\alpha$, $\ddot{\blacksquare} = \partial^2\blacksquare/\partial t^2$, τ_{ij} are the components of the stress tensor, and f_i are the components of the external body force vector.

To get insight into the fact that the classical elasticity tensor is achiral, the fourth-rank elasticity tensor C_{ijkl} is transformed to a rank-two elasticity tensor $C_{\alpha\beta}$ by employing the following kinematical fields of the 2D isotropic solid (Scheibner et al., 2020):

$$\begin{aligned} \gamma_1 &= u_{x,x} + u_{y,y} \\ \gamma_2 &= u_{x,y} - u_{y,x} \\ \gamma_3 &= u_{x,x} - u_{y,y} \\ \gamma_4 &= u_{x,y} + u_{y,x} \end{aligned} \tag{2}$$

where the 2D isotropic solid can exhibit deformations including dilations (volumetric strains) γ_1 and γ_3, rotation γ_2, and shear γ_4. Classical elasticity assumes the existence of a free energy function of γ_1, γ_2, γ_3, and γ_4 such that the energy per unit volume w can be expressed, as follows:

$$w = \frac{1}{4}\left(\hat{B}_1\gamma_1^2 + \hat{C}\gamma_2^2 + \hat{B}_2\gamma_3^2 + \hat{\mu}\gamma_4^2\right) \tag{3}$$

where $\hat{B}_1$ and $\hat{B}_2$ are bulk elastic moduli of the volumetric straining of the solid with γ_1 and γ_3, respectively, while $\hat{C}$ and $\hat{\mu}$ are torsional and shear elastic moduli, respectively.

According to Eq. (3), the constitutive law can be obtained in the following form $\sigma_\alpha = C_{\alpha\beta}\gamma_\beta$, where $\sigma_\alpha = 2\partial w/\partial\gamma_\alpha$

$$\begin{Bmatrix} \sigma_1 \\ \sigma_2 \\ \sigma_3 \\ \sigma_4 \end{Bmatrix} = \begin{bmatrix} \hat{B}_1 & 0 & 0 & 0 \\ 0 & \hat{C} & 0 & 0 \\ 0 & 0 & \hat{B}_2 & 0 \\ 0 & 0 & 0 & \hat{\mu} \end{bmatrix} \begin{Bmatrix} \gamma_1 \\ \gamma_2 \\ \gamma_3 \\ \gamma_4 \end{Bmatrix}, \ i.e., \ \sigma_\alpha = C_{\alpha\beta}\gamma_\beta \tag{4}$$

The stress vector σ_α in Eq. (4) can be related to the stress tensor τ_{ij}, as follows:

$$\begin{aligned} \sigma_1 &= \tau_{xx} + \tau_{yy} \\ \sigma_2 &= \tau_{yx} - \tau_{xy} \\ \sigma_3 &= \tau_{xx} - \tau_{yy} \\ \sigma_4 &= \tau_{xy} + \tau_{yx} \end{aligned} \tag{5}$$

The 2D elasticity tensor $C_{\alpha\beta}$ in Eq. (4) is achiral, as its parity inversion is equal to its rotation in the spatial space. This can be verified by inverting the elasticity tensor $C_{\alpha\beta}$ about one spatial coordinate (Scheibner et al., 2020), where $C_{\alpha\beta}$ being a diagonal tensor is the same before and after the spatial inversion.

The elasticity tensor $C_{\alpha\beta}$ can be chiral when coupling is realized between two different kinematical fields. For 2D isotropic solids, coupling can be achieved between dilation γ_1 and rotation γ_2 and between dilation γ_3 and shear γ_4 such that the energy density function w becomes:

$$w = \tfrac{1}{4}\left(\hat{B}_1\gamma_1^2 + \hat{C}\gamma_2^2 + \hat{B}_2\gamma_3^2 + \hat{\mu}\gamma_4^2 + 2\hat{A}\gamma_1\gamma_2 + 2\hat{K}\gamma_3\gamma_4\right) \tag{6}$$

where $\hat{A}$ is an elastic modulus of dilation–rotation coupling, and $\hat{K}$ is an elastic modulus of dilation–shear coupling. Accordingly, the constitutive law $\sigma_\alpha = C_{\alpha\beta}\gamma_\beta$ can be obtained, and thus the elasticity tensor $C_{\alpha\beta}$ becomes:

$$C_{\alpha\beta} = \begin{bmatrix} \hat{B}_1 & \hat{A} & 0 & 0 \\ \hat{A} & \hat{C} & 0 & 0 \\ 0 & 0 & \hat{B}_2 & \hat{K} \\ 0 & 0 & \hat{K} & \hat{\mu} \end{bmatrix} \tag{7}$$

According to the chiral elasticity tensor shown in Eq. (7), the chiral modulus $\hat{A}$ enables dilatational deformations when the chiral solid is subjected to torques/rotations, and rotations when the solid is subject to applied pressure/dilation, while the chiral modulus $\hat{K}$ enables shear deformations due to normal stresses/strains and normal strains due to shear stresses/strains. Importantly, these chiral deformations are reciprocal, meaning that – for example – if dilatational deformation D_1 resulted from an applied rotation R_1, the same rotation R_1 would result from an applied dilatational deformation D_1.

The chirality of the elasticity tensor $C_{\alpha\beta}$ in Eq. (7) can be verified by implementing inversion and rotation of the tensor about one spatial coordinate, e.g., x-axis. After the inversion about x-axis $C_{\alpha\beta} \rightarrow P_{\alpha r}C_{rq}P_{q\beta}$, $C_{\alpha\beta}$ becomes:

$$C_{\alpha\beta} = \begin{bmatrix} \hat{B}_1 & -\hat{A} & 0 & 0 \\ -\hat{A} & \hat{C} & 0 & 0 \\ 0 & 0 & \hat{B}_2 & -\hat{K} \\ 0 & 0 & -\hat{K} & \hat{\mu} \end{bmatrix} \tag{8}$$

while after the rotation about x-axis $C_{\alpha\beta} \rightarrow R_{\alpha r}C_{rq}R_{q\beta}$, $C_{\alpha\beta}$ becomes:

$$C_{\alpha\beta} = \begin{bmatrix} \hat{B}_1 & \hat{A} & 0 & 0 \\ \hat{A} & \hat{C} & 0 & 0 \\ 0 & 0 & \hat{B}_2 + t & \hat{K} + d \\ 0 & 0 & \hat{K} + d & \hat{\mu} - t \end{bmatrix} \tag{9}$$

where

$$P_{\alpha\beta} = \begin{bmatrix} 1 & 0 & 0 & 0 \\ 0 & -1 & 0 & 0 \\ 0 & 0 & 1 & 0 \\ 0 & 0 & 0 & -1 \end{bmatrix}, \quad R_{\alpha\beta} = \begin{bmatrix} 1 & 0 & 0 & 0 \\ 0 & 1 & 0 & 0 \\ 0 & 0 & \cos\theta & \sin\theta \\ 0 & 0 & -\sin\theta & \cos\theta \end{bmatrix}$$
$$t = -\left(\left(\hat{B}_2 - \hat{\mu}\right)\sin^2\theta \; - 2\hat{K}\cos\theta \, \sin\theta \;\right)$$
$$d = -\left(\left(\hat{B}_2 - \hat{\mu}\right)\cos\theta \, \sin\theta \; + 2\hat{K}\sin^2\theta \;\right) \tag{10}$$

According to Eqs. (8) and (9), the elasticity tensor $C_{\alpha\beta}$ is achiral if and only if $\hat{A} = 0$ and $\hat{K} = -d/2$, and it is chiral otherwise.

2.2. Chiral, nonreciprocal elasticity tensor

As discussed above, the elasticity tensor in Eq. (7) is chiral, except for specific values of the chiral elastic constants $\hat{A}$ and $\hat{K}$. In this section, we propose a novel form of the elasticity tensor that captures the coupled effects of chirality with nonreciprocity. Recently, the concept of nonreciprocal elasticity (Shaat, 2020) was introduced to demonstrate a new class of elastic materials that can modulate their elastic properties depending on the direction of the applied load/deformation. Therefore, these materials can break both time-reversal symmetry and deformation symmetry of various physical systems (Coulais et al., 2017; Asadchy et al., 2020). Fig. 1(a) shows an illustration of this *directional nonreciprocal elasticity*, where the elastic modulus of the material is different when inverting the applied force/deformation along the same direction. The verification of the directional nonreciprocity can be done by acting on the material with a deformation field that is spatially inverted, while measuring the elastic modulus/stiffness of the solid material before and after the inversion of the deformation field. The material is reciprocal if the elastic modulus is the same before and after the field inversion, and it is nonreciprocal otherwise.

Here, we propose a new type of nonreciprocity that is distinct from the aforementioned directional nonreciprocity through the coupling with chirality. This new "*chiral, nonreciprocal elasticity*" depends on the coupling between two different deformation fields, and thus for 2D isotropic solids it is contingent on chirality. The chiral, nonreciprocal elasticity can be realized by adding

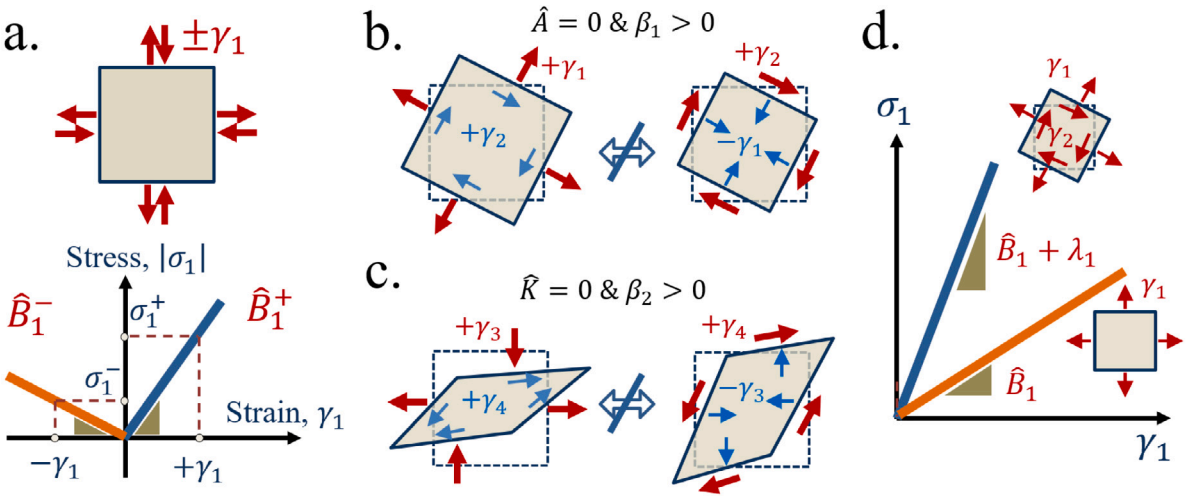

Fig. 1. The concept of Chiral, Nonreciprocal Elasticity. (a) Illustration of directional nonreciprocity. A solid material is tested under spatially inverted dilation (volumetric strain) $\pm\gamma_1$, where the elastic modulus $B_1^{\pm} = \sigma_1^{\pm}/\pm\gamma_1$ is different when inverting the applied strain $\pm\gamma_1$. (b) and (c) Illustration of Form I of chiral nonreciprocity. (b) The elastic modulus β_1 achieves non-symmetric coupling between dilation γ_1 and rotation γ_2, where the positive dilation $+\gamma_1$ causes positive rotation $+\gamma_2$ (left), while the positive rotation $+\gamma_2$ causes negative dilation $-\gamma_1$ (right). (c) The elastic modulus β_2 achieves non-symmetric coupling between dilation γ_3 and shear γ_4, where the positive dilation $+\gamma_3$ causes positive shear $+\gamma_4$ (left), while the positive shear $+\gamma_4$ causes negative dilation $-\gamma_3$ (right). (d) Illustration of Form II of chiral nonreciprocity. A chiral, nonreciprocal elastic solid is tested under dilation γ_1, where the elastic modulus is $\hat{B}_1 = \sigma_1/\gamma_1$ when acting on the solid with dilation γ_1 only, while it becomes $\hat{B}_1 + \lambda_1$ when acting on the solid with both dilation γ_1 and rotation γ_2.

nonreciprocity to a chiral solid, such that the chiral elasticity tensor $C_{\alpha\beta}$ in Eq. (7) is modified, and thus the constitutive law $\sigma_\alpha = C_{\alpha\beta}\gamma_\beta$ becomes:

$$\begin{Bmatrix} \sigma_1^{\pm} \\ \sigma_2^{\pm} \\ \sigma_3^{\pm} \\ \sigma_4^{\pm} \end{Bmatrix} = \begin{bmatrix} \hat{B}_1^{\pm} + \lambda_1^{\pm} & \hat{A}^{\pm} + \beta_1^{\pm} & 0 & 0 \\ \hat{A}^{\pm} - \beta_1^{\pm} & \hat{C}^{\pm} + \lambda_2^{\pm} & 0 & 0 \\ 0 & 0 & \hat{B}_2^{\pm} + \lambda_3^{\pm} & \hat{K}^{\pm} + \beta_2^{\pm} \\ 0 & 0 & \hat{K}^{\pm} - \beta_2^{\pm} & \hat{\mu}^{\pm} + \lambda_4^{\pm} \end{bmatrix} \begin{Bmatrix} \pm\gamma_1 \\ \pm\gamma_2 \\ \pm\gamma_3 \\ \pm\gamma_4 \end{Bmatrix} \tag{11}$$

where the superscripts '$\pm$' indicate the change in the elastic modulus value by the spatial inversion of the applied load or deformation acting on the solid. $\lambda_i \to \lambda_1$, λ_2, λ_3, and λ_4 and $\beta_i \to \beta_1$ and β_2 are elastic moduli that appear in the elasticity tensor after the addition of nonreciprocity. In the rest of the paper, the superscripts '$\pm$' are eliminated for writing convenience, while accounting for the change in values of the elastic moduli upon changing the direction of the applied stress/deformation.

2.2.1. *First form of chiral, nonreciprocal elasticity*

In addition to the direction-dependence of the elastic moduli, the elasticity tensor in Eq. (11) indicates two forms of chiral, nonreciprocal elasticity. The first form of chiral, nonreciprocal elasticity (Form I) can be defined by the contrast in the elastic moduli of the chiral coupling between two deformation fields, and this – in turn – makes the elasticity tensor $C_{\alpha\beta}$ asymmetric as its skew-symmetric part depends on the moduli β_1 and β_2. For instance, in Eq. (11), the dilation γ_1 is coupled with the rotation γ_2 such that the dilatational stress σ_1 can produce rotation, and the torsional stress σ_2 can produce dilation. If the elastic modulus of rotation due to σ_1 is the same as the elastic modulus of the dilation due to σ_2 (*the coupling elastic modulus is the same*), the elastic solid is reciprocal, while it is nonreciprocal otherwise. The parameter β_1 is an elastic modulus of nonreciprocal dilation–rotation coupling, as the positive dilation causes a positive rotation, while – in contrast – the positive rotation gives a negative dilation, when $\hat{A} = 0$ and $\beta_1 > 0$ (Fig. 1(b)). Similarly, the parameter β_2 is an elastic modulus of nonreciprocal dilation–shear coupling, as the positive dilation causes a positive shear, while – in contrast – the positive shear gives a negative dilation, when $\hat{K} = 0$ and $\beta_2 > 0$ (Fig. 1(c)). Beyond these extreme cases, at which the chiral moduli $\hat{A}$ and $\hat{K}$ are zero, the behavior of a real chiral solid such as the one proposed later in this paper may require $\hat{A} \neq 0$ and $\hat{K} \neq 0$, while the nonreciprocal behavior is still maintained by having the moduli $\beta_1 \neq 0$ and $\beta_2 \neq 0$, in which the dilation–rotation coupling or the dilation–shear coupling is in general nonreciprocal. The verification of this form of chiral nonreciprocity can be done by deforming the chiral solid with only one of the two coupled deformation fields at a time while measuring the contrast in the coupling modulus when changing the applied deformation field.

2.2.2. *Second form of chiral, nonreciprocal elasticity*

Solids are often deformed through the application of different deformation fields, which can be coupled if the solid is chiral. Therefore, we anticipate situations where the elastic moduli of the solid may change depending on how many coupled deformation fields are applied. This gives the second form of chiral nonreciprocal elasticity (Form II), which can be defined by the change in the

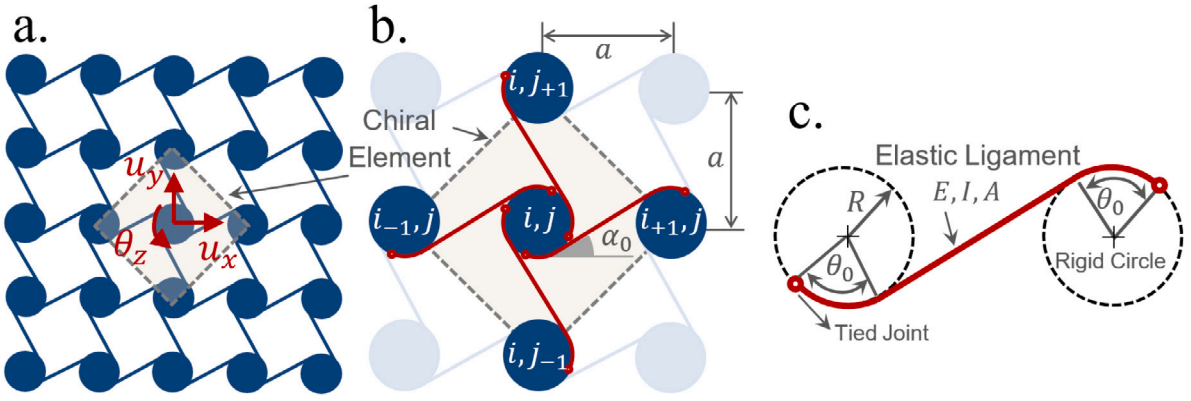

Fig. 2. Chiral, nonreciprocal elastic 2D metamaterial made of passive chiral elements. (a) The lattice structure of the chiral metamaterial. The circles are rigid particles that exhibit three degrees of freedom u_x, u_y, and θ_z and are connected by elastic ligaments that can stretch and bend. (b) The Chiral element of the 2D metamaterial, which consists of a central rigid circle connected to four other rigid circles via four solid, elastic ligaments. The chirality is achieved by the chiral distribution of the ligaments around the central circle. (c) The geometry of the elastic ligament that enables local geometrical asymmetry and nonreciprocity of the chiral metamaterial.

elastic modulus of the solid depending on whether it is deformed with only one deformation field or multiple deformation fields (Fig. 1(d)). For instance, due to the dilation–rotation coupling, we anticipate that the dilatational modulus $\hat{B}_1$ varies depending on the following two scenarios: (1) we act on the chiral solid with dilation alone (i.e., $\gamma_1 \neq 0$ but $\gamma_2 = 0$), and (2) the chiral solid is pre-deformed by rotation $\gamma_2 \neq 0$, while we act on it with dilation γ_1. In the first scenario, where only dilation γ_1 is applied, the dilatational stress $\sigma_1 \propto \gamma_1$, and the constant of proportionality is the elastic modulus $\hat{B}_1$ (i.e., $\sigma_1 = \hat{B}_1\gamma_1$). In the second scenario, where the chiral solid is pre-deformed by rotation γ_2, the constant of $\sigma_1 - \gamma_1$ proportionality is changed to become $\hat{B}_1 + \lambda_1$, where λ_1 is the change in the dilatational modulus between the two scenarios. Thus, the modulus λ_1 is developed only when the chiral solid is pre-deformed by rotation while acting on it with dilation. Similarly, the modulus λ_2 is developed when we act on the chiral solid with rotation, while the solid is pre-deformed by dilation. In the constitutive law in Eq. (11), the elastic moduli λ_i are developed only when the isotropic chiral solid is deformed by two different, but coupled, deformation fields. We emphasize that the described constitutive behavior of the chiral, nonreciprocal elastic solids is still within the context of linear elasticity, as the stress is a linear function of the deformation, though the system is nonlinear as the elastic constants of the constitutive model in Eq. (11) change depending on (1) the direction of the applied deformation (not the value of the deformation), and (2) whether the solid is subject to coupled deformation fields or not.

3. Chiral, nonreciprocal elastic 2D isotropic metamaterial made of passive chiral elements

Having proposed chiral, non-reciprocal elasticity in the form of the elasticity tensor in Eq. (11), the question remains—what does a solid that exhibits that constitutive behavior look like? Odd elastic solids have been recently developed to describe a class of solid materials with non-symmetric elasticity (Scheibner et al., 2020; Chen et al., 2021b; Brandenbourger et al., 2022). This route of obtaining non-symmetric elasticity depends on using active energy sources at the solid's microstructure, where current designs of odd elastic solids utilize active elements operating under thermodynamic non-equilibrium, which requires the presence of independent (external) energy sources to actuate and control the motion of the internal active components. For instance, piezoelectric actuators operated by external energy sources along with feed-forward controllers were used to realize odd elastic, active meta-beams, which achieved non-symmetric elasticity (Chen et al., 2021b). Similarly, circular arrays of active joints with externally powered motors and micro-controllers were used to realize autonomous, active robots with non-symmetric elastic response (Brandenbourger et al., 2022). Given this need for active elements and energy sources, the development of metamaterials with non-symmetric elasticity using only passive elements that do not require external sources of energy to operate has been out of reach. Here, we resolve this challenge and demonstrate a 2D isotropic metamaterial that is made entirely from *passive chiral elements* and is capable of developing a non-symmetric elastic response enabled by the chiral, nonreciprocal elasticity described above and without any external energy sources. The metamaterial is chiral, and thus it can achieve coupling between different deformation fields, while, to enable nonreciprocity, the chiral metamaterial is made with local (microscopic) geometrical asymmetry (Fig. 2).

The specific structure of the considered chiral metamaterial is shown in Fig. 2(a), which is a 2D lattice of chiral elements, each of which consists of a central rigid circle that is connected to other four rigid circles by four elastic ligaments (Fig. 2(b)). The local geometrical asymmetry of the considered chiral metamaterial is manifested in the ligaments being made with curved portions at their ends, and thus the ligaments are curved around the rigid circles, as shown in Fig. 2(c). The geometrical asymmetry is defined by the geometrical angle θ_0 such that when $\theta_0 = 0$, the ligaments are straight (without curved ends) and tangent to the rigid circles, and thus the chiral metamaterial has no asymmetries and becomes reciprocal. The rigid circle possesses three kinematical degrees of freedom, i.e. two displacements u_x and u_y and rotation (spin) about its center θ_z, and the ligaments are elastic (Bernoulli–Euler) beams that can stretch and bend, with elastic modulus E, area moment of inertia I, and cross-sectional area A, and thus the chiral element is

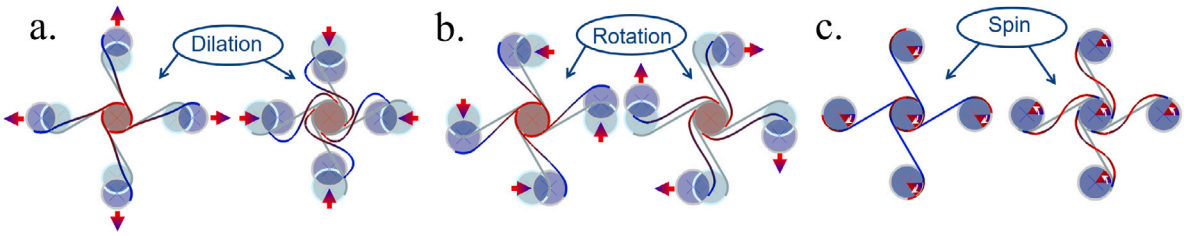

Fig. 3. Nonreciprocal deformation fields of the chiral element. Spatially inverted (a) dilation $\pm\gamma_1$, (b) rotation $\pm\gamma_2$, and (c) spin $\pm\theta_z$ of the chiral element. In (a) and (b), the rigid circles translate but do not spin. In (c), all circles are only spin with θ_z. All figures obtained through finite element simulations using ABAQUS.

comprised only of passive components. Two parameters define the chiral geometry of the metamaterial; the chiral angle α_0 and the lattice length a, where the radius of the circle $R = (a/2)\sin\alpha_0$, and the length of the straight portion of the ligament $L = a\cos\alpha_0$ (Fig. 2). It is important to note that the ligaments are stress-free in the initial curved configuration shown in Fig. 2(c). Furthermore, the ligaments are fixed to the circles at only one point, the tied joints labeled in Fig. 2(c). As the chiral metamaterial is subject to deformation, the ligaments are allowed to either wrap further around or deform away from the circles. Further attachment to the circles are modeled using normal contact forces; there are no tangential, or dissipative frictional contact forces that are considered.

The chiral metamaterial enables asymmetric elasticity by replacing the active elements that have been used in current designs of odd elastic, active solids (Scheibner et al., 2020; Chen et al., 2021b) with the chiral element shown in Fig. 2(b), which behaves in a chiral, nonreciprocal elastic fashion. By means of finite element simulations using the commercial simulation package ABAQUS (Smith, 2009), the mechanism enabling chiral, nonreciprocal elastic behavior of the chiral element is demonstrated in Fig. 3 for different deformation modes. In all cases, enabled by the geometrical asymmetry, certain directions of deformation enable stiffening by pulling the elastic ligaments tighter and straighter around the rigid circles, whereas other directions of deformation enable softening by causing the elastic ligaments to detach from the rigid circles by becoming more curved. For concreteness, consider the case of dilation in Fig. 3(a). There, positive dilation results in the stretching of the elastic ligaments, and thus the curved ends of the ligament come into contact with the circles, resulting in a relatively stiff mechanical response. In contrast, if negative dilation is prescribed, the elastic ligaments may, except for the fixed points, detach from the rigid circles, while becoming more curved, resulting in a relatively soft mechanical response. Thus, the chiral element exhibits two different stiffness values depending on the direction of the applied loading. The same mechanism can be observed in Figs. 3(b) and 3(c) depending on the direction of applied loading, resulting in the nonreciprocal elastic response that we aim to capture, below, using a chiral, nonreciprocal elasticity tensor.

We emphasize that each ligament in the chiral element is a passive, elastic component that conserves energy when deformed in isolation from the chiral structure. Each circle is also a passive component that rigidly moves. However, when the curved ligament is tied to and comes into contact with the rigid circles, the result is a structure of multiple passive components (see Fig. 2(b)), which behaves in a chiral, nonreciprocal elastic fashion, and thus this minimal structure enables asymmetric elasticity of the chiral metamaterial. The chiral, nonreciprocal elasticity of the chiral metamaterial emerges due to (1) the chiral distribution of the ligaments around the rigid circles, and (2) the nonreciprocity enabled by making the ends of the ligaments curved. Thus, if the ligaments are not curved or are not chiral with respect to the circles, the chiral, nonreciprocal elasticity is suppressed.

Remark 1. Microscopic geometrical asymmetries in elastic media such as the curved ligaments in Fig. 2(c) enable the elasticity and the nonreciprocal behavior of the solid to differ depending on how it is deformed. Therefore, it becomes crucial to know a priori what nonreciprocal behavior and its associated deformations are going to be considered when determining the continuum field equations and the constitutive model of the nonreciprocal elastic solid. As our objective is to reveal the chiral, nonreciprocal elasticity of the chiral metamaterial, here we focus on the global nonreciprocal behavior of the chiral metamaterial by considering the specific class of deformations which satisfy the following conditions. First, those which make the mechanical response of the chiral metamaterial be isotropic. Second, those which make the stress a linear function of the strain only. Third, those which ensure that the chiral metamaterial conserves linear momentum.

3.1. Constitutive modeling

Having established the physical mechanisms, as shown in Figs. 2 and 3, enabling the emergence of nonreciprocal elastic behaviors, we now show the formalism of the continuum constitutive model of the chiral, nonreciprocal elasticity of the considered chiral metamaterial. Because an asymmetric elastic response cannot emerge from a free energy function (Scheibner et al., 2020), we develop a discrete model of the chiral element highlighted in Fig. 2(b) based on Newtonian mechanics, from which we determine the equivalent, elastic continuum field equations of the chiral metamaterial, and then the constitutive model of the chiral, nonreciprocal elasticity. Specifically, we determine the equations of motion and the constitutive relationships of the chiral metamaterial under deformations that satisfy the conditions stated above in Remark 1. To have the stress be proportional to strain, which is required

to conserve linear momentum, we assume homogeneous deformation of all ligaments, i.e. all ligaments along the same direction exhibit similar deformations. Isotropy requires that the chiral metamaterial exhibits the same stiffness along different axes, which also requires that the chiral metamaterial should exhibit a uniform stiffness for all ligaments for a given mode of deformation. Examples of deformations that satisfy these conditions are shown in Fig. 3, where all ligaments of the chiral element are either compressed or stretched depending on the direction of the applied deformation.

3.1.1. Discrete, Newtonian mechanics

We consider the chiral element shown in Fig. 2(b) in which each circle is a rigid particle of mass m and mass rotatory inertia J that possesses three kinematical degrees of freedom, i.e., u_x, u_y and θ_z, while the ligaments are Bernoulli–Euler beams. The rotation of the circle θ_z is a spin field that is distinct from the rotation $(u_{x,y}-u_{y,x})$ that would be applied at the external boundary of the chiral element, as illustrated by comparing Figs. 3(b) and 3(c). Interaction forces and couples are developed between the rigid circles that move and rotate through the elastic ligaments that bend and stretch, such that the forces and couples of interactions between the central circle i,j and one of its neighbor circles q can be determined in the form:

$$\begin{Bmatrix} F_x^l \\ F_y^l \\ M_z^l \end{Bmatrix} = \begin{bmatrix} k_{xx}^l & k_{xy}^l & k_{x\theta}^l \\ k_{yx}^l & k_{yy}^l & k_{y\theta}^l \\ k_{\theta x}^l & k_{\theta y}^l & k_{\theta\theta}^l \end{bmatrix} \begin{Bmatrix} u_x^{i,j} - u_x^q \\ u_y^{i,j} - u_y^q \\ \theta_z^{i,j} + \theta_z^q \end{Bmatrix} \tag{12}$$

where $k_{\alpha\beta}^l$ are the various equivalent stiffnesses of the ligament l that connects the central circle i,j and its neighbor circle q. The stiffnesses $k_{\alpha\beta}^l$ can be related to the generalized rigidities of the ligament, as follows:

$$\begin{aligned}
k_{xx}^l &= S_{\hat{x}\hat{x}}^l \cos^2\alpha^l + S_{\hat{y}\hat{y}}^l \sin^2\alpha^l - (S_{\hat{x}\hat{y}}^l + S_{\hat{y}\hat{x}}^l)\sin\alpha^l \cos\alpha^l \\
k_{yy}^l &= S_{\hat{x}\hat{x}}^l \sin^2\alpha^l + S_{\hat{y}\hat{y}}^l \cos^2\alpha^l + (S_{\hat{x}\hat{y}}^l + S_{\hat{y}\hat{x}}^l)\sin\alpha^l \cos\alpha^l \\
k_{xy}^l &= \left(S_{\hat{x}\hat{x}}^l - S_{\hat{y}\hat{y}}^l\right)\sin\alpha^l \cos\alpha^l + S_{\hat{x}\hat{y}}^l \cos^2\alpha^l - S_{\hat{y}\hat{x}}^l \sin^2\alpha^l \\
k_{yx}^l &= \left(S_{\hat{x}\hat{x}}^l - S_{\hat{y}\hat{y}}^l\right)\sin\alpha^l \cos\alpha^l + S_{\hat{y}\hat{x}}^l \cos^2\alpha^l - S_{\hat{x}\hat{y}}^l \sin^2\alpha^l \\
k_{x\theta}^l &= S_{\hat{x}\theta}^l \cos\alpha^l - S_{\hat{y}\theta}^l \sin\alpha^l \\
k_{\theta x}^l &= S_{\theta\hat{x}}^l \cos\alpha^l - S_{\theta\hat{y}}^l \sin\alpha^l \\
k_{y\theta}^l &= S_{\hat{x}\theta}^l \sin\alpha^l + S_{\hat{y}\theta}^l \cos\alpha^l \\
k_{\theta y}^l &= S_{\theta\hat{x}}^l \sin\alpha^l + S_{\theta\hat{y}}^l \cos\alpha^l \\
k_{\theta\theta}^l &= S_{\theta\theta}^l
\end{aligned} \tag{13}$$

where α^l is the chiral angle of ligament l measured from the $+x-$direction and $S_{\hat{\alpha}\hat{\beta}}^l$ are the various rigidities of the ligament l that are defined with respect to the ligament's local coordinates $(\hat{x},\hat{y})$. Because the ligament is modeled as a Bernoulli–Euler beam, it has axial rigidity $S_{\hat{x}\hat{x}}$, bending rigidity $S_{\hat{y}\hat{y}}$, rotational rigidity $S_{\theta\theta}$, and rigidity for bending-rotation coupling $S_{\hat{y}\theta}$ and $S_{\theta\hat{y}}$, while because the ends of the ligament are curved, it also has rigidities for axial-bending coupling $S_{\hat{x}\hat{y}}$ and $S_{\hat{y}\hat{x}}$ and axial-rotation coupling $S_{\hat{x}\theta}$ and $S_{\theta\hat{x}}$. It should be noted that, due to the geometrical asymmetry of the ligaments, the rigidity matrix $S_{\hat{\alpha}\hat{\beta}}$ and the equivalent stiffness matrix $k_{\alpha\beta}$ are – in general – asymmetric (i.e., $S_{\hat{\alpha}\hat{\beta}} \neq S_{\hat{\beta}\hat{\alpha}}$ and $k_{\alpha\beta} \neq k_{\beta\alpha}$), as the rigidity of the ligament varies depending on the deformation of the chiral element—specifically, whether the ligaments are firmly attached to or detached from the circles during the deformation of the chiral element as illustrated in Fig. 3.

The equations of motion of the central circle i,j can be determined according to the defined interactions with the nearest-neighbor circles (Eq. (12)), as follows:

$$\begin{aligned}
\sum_{l=1}^{4} F_x^l &= -m\ddot{u}_x^{i,j} \\
\sum_{l=1}^{4} F_y^l &= -m\ddot{u}_y^{i,j} \\
\sum_{l=1}^{4} M_z^l &= -J\ddot{\theta}_z^{i,j}
\end{aligned} \tag{14}$$

By observing that $\alpha^{l=1} = \alpha_0$, $\alpha^{l=2} = \alpha_0 + 90°$, $\alpha^{l=3} = \alpha_0 + 180°$, $\alpha^{l=4} = \alpha_0 + 270°$ and considering the stiffnesses defined in Eq. (13), while also considering that all ligaments are identical and exhibit similar deformations, the balance of forces along x- and y-directions and the moment about z-direction (Eq. (14)) can be explicitly written in the form:

$$\begin{aligned}
&m\ddot{u}_x^{i,j} + k_{xx}\left(2u_x^{i,j} - u_x^{i+1,j} - u_x^{i-1,j}\right) + k_{xy}\left(2u_y^{i,j} - u_y^{i+1,j} - u_y^{i-1,j}\right) - k_{x\theta}\left(\theta_z^{i-1,j} - \theta_z^{i+1,j}\right) \\
&+k_{yy}\left(2u_x^{i,j} - u_x^{i,j+1} - u_x^{i,j-1}\right) - k_{yx}\left(2u_y^{i,j} - u_y^{i,j+1} - u_y^{i,j-1}\right) + k_{y\theta}\left(\theta_z^{i,j-1} - \theta_z^{i,j+1}\right) = 0
\end{aligned} \tag{15}$$

$$\begin{aligned}
&m\ddot{u}_y^{i,j} + k_{yx}\left(2u_x^{i,j} - u_x^{i+1,j} - u_x^{i-1,j}\right) + k_{yy}\left(2u_y^{i,j} - u_y^{i+1,j} - u_y^{i-1,j}\right) - k_{y\theta}\left(\theta_z^{i-1,j} - \theta_z^{i+1,j}\right) \\
&-k_{xy}\left(2u_x^{i,j} - u_x^{i,j+1} - u_x^{i,j-1}\right) + k_{xx}\left(2u_y^{i,j} - u_y^{i,j+1} - u_y^{i,j-1}\right) - k_{x\theta}\left(\theta_z^{i,j-1} - \theta_z^{i,j+1}\right) = 0
\end{aligned} \tag{16}$$

$$\begin{aligned}
&J\ddot{\theta}_z^{i,j} + k_{\theta x}\left(u_x^{i-1,j} - u_x^{i+1,j} + u_y^{i,j-1} - u_y^{i,j+1}\right) + k_{\theta y}\left(u_y^{i-1,j} - u_y^{i+1,j} + u_x^{i,j+1} - u_x^{i,j-1}\right) \\
&+k_{\theta\theta}\left(4\theta_z^{i,j} + \theta_z^{i,j+1} + \theta_z^{i,j-1} + \theta_z^{i+1,j} + \theta_z^{i-1,j}\right) = 0
\end{aligned} \tag{17}$$

Because of the geometrical asymmetry of the chiral element that is manifested in the ligaments being curved around the circles, the behavior of the chiral element is chiral nonreciprocal. To demonstrate the chiral nonreciprocity of the element, the equivalent stiffnesses $k_{\alpha\beta}$ in Eqs. (15)–(17) were numerically determined by finite element simulations (Smith, 2009) (see Appendix A for more details). Specifically, because the ligaments are identical and exhibit similar deformations, we considered one ligament connecting two circles (Fig. 2(c)) of a chiral element with chiral angle $\alpha_0 = 30°$ and lattice length $a = 20$ mm, where the circles are rigid and the ligament is made of Aluminum (with elastic modulus $E = 70$ GPa) with 1.5 mm thickness and 30 mm width. The ligament is curved at its ends to achieve a geometrical asymmetry with $\theta_0 = 60°$. The ligament connecting two circles was considered under the various deformation fields shown in Fig. 3, while the equivalent stiffnesses $k_{\alpha\beta}$ were determined by calculating the slopes of the numerically determined force–deformation curves. The equivalent stiffnesses were obtained depending on (1) the direction of the applied deformation field, revealing directional nonreciprocity (Fig. 1(a)), and (2) whether the ligament is deformed by two coupled deformation fields or not, revealing Form II of chiral nonreciprocity (Fig. 1(d)), while also, the stiffness matrix was obtained non-symmetric, as shown in Table A.1 of Appendix A such that $k_{\alpha\beta} \neq k_{\beta\alpha}$, which indicates Form I of chiral nonreciprocity (Figs. 1(b) and 1(c)). These stiffnesses will be used in the next section to evaluate the continuum elastic moduli for the chiral, nonreciprocal elasticity.

3.1.2. Continuum field equations

In order to study the chiral, nonreciprocal constitutive behavior of the chiral metamaterial, the continuum field equations are determined based on the discrete equations of motion in Eqs. (15)–(17). By implementing Taylor expansions $\varrho^{i\pm1,j} \approx \varrho(x,y) \pm a(\partial\varrho(x,y)/\partial x) + \left(a^2/2\right)\left(\partial^2\varrho(x,y)/\partial x^2\right)$ and $\varrho^{i,j\pm1} \approx \varrho(x,y) \pm a(\partial\varrho(x,y)/\partial y) + \left(a^2/2\right)\left(\partial^2\varrho(x,y)/\partial y^2\right)$, where ϱ denotes a degree of freedom, i.e., u_x, u_y, and θ_z, the discrete equations of motion (Eqs. (15)–(17)) can be written at the continuum limit such that $\varrho^{i,j} \approx \varrho(x,y)$, as follows:

$$\hat{B}u_{x,xx} + \hat{C}u_{x,yy} + \hat{\xi}_1 u_{y,xx} - \hat{\xi}_2 u_{y,yy} + \hat{C}\theta_{z,y} - \hat{\xi}_1\theta_{z,x} = \hat{\rho}\ddot{u}_x \tag{18}$$

$$\hat{B}u_{y,yy} + \hat{C}u_{y,xx} + \hat{\xi}_2 u_{x,xx} - \hat{\xi}_1 u_{x,yy} - \hat{C}\theta_{z,x} - \hat{\xi}_1\theta_{z,y} = \hat{\rho}\ddot{u}_y \tag{19}$$

$$\hat{C}\left(u_{y,x} - u_{x,y}\right) + \hat{\xi}_2\left(u_{x,x} + u_{y,y}\right) - 2\hat{C}\theta_z + \hat{\chi}\left(\theta_{z,xx} + \theta_{z,yy}\right) = \hat{J}\ddot{\theta}_z \tag{20}$$

where $\hat{\rho}$ is the mass density, and $\hat{J}$ is the mass rotatory inertia. The material coefficients in Eqs. (18)–(20) are defined in terms of the equivalent stiffnesses of the ligaments, as follows:

$$\hat{B} = \frac{k_{xx}}{4b}, \hat{C} = \frac{k_{yy}}{4b} = \frac{k_{\theta y}}{2ab} = \frac{k_{y\theta}}{2ab} = \frac{k_{\theta\theta}}{a^2 b}, \hat{\chi} = -\frac{k_{\theta\theta}}{2b}, \hat{\xi}_1 = \frac{k_{xy}}{4b} = \frac{k_{x\theta}}{2ab}, \hat{\xi}_2 = \frac{k_{yx}}{4b} = \frac{k_{\theta x}}{2ab} \tag{21}$$

where a is the lattice constant and b is the ligament width. It should be noted that, after the inspection of the equivalent stiffness of the chiral element, it is found that $k_{y\theta} \cong k_{\theta y}$, $k_{xy}/4b \cong k_{x\theta}/2ab$, and $k_{yx}/4b \cong k_{\theta x}/2ab$. In Eqs. (18)–(20), $\hat{B}$ is the bulk elastic modulus, and $\hat{C}$ is the torsional elastic modulus, while the coefficients $\hat{\xi}_1$ and $\hat{\xi}_2$ are chiral elastic moduli, which appear in the equations of motion if and only if the solid is chiral, as these moduli vanish when $\alpha_0 = 0$.

As the equivalent stiffness of the chiral element is asymmetric, i.e., $k_{\alpha\beta} \neq k_{\beta\alpha}$, the chiral elastic moduli $\hat{\xi}_1$ and $\hat{\xi}_2$ are not equal (see Eq. (21)), and this enables asymmetric elasticity of the chiral metamaterial (Form I of chiral, nonreciprocal elasticity), which we aim to demonstrate next. Furthermore, because the values of the equivalent stiffness of the chiral element $k_{\alpha\beta}$ change due to chiral nonreciprocity, the values of the various elastic moduli shown in Eqs. (18)–(20) also change by (1) the spatial inversion of the applied deformation field (directional nonreciprocity), as well as (2) acting on the chiral metamaterial with coupled deformation fields (Form II of chiral nonreciprocity). By introducing the coefficients λ_i and κ_i that measure the modulation of the elastic moduli due to Form II of chiral nonreciprocity, while accounting for the modulation of the elastic moduli due to directional nonreciprocity, Eqs. (18)–(20) take the following form:

$$(\hat{B} + \lambda_1)u_{x,xx} + (\hat{C} + \lambda_2)u_{x,yy} + (\hat{\xi}_1 + \kappa_1)u_{y,xx} - (\hat{\xi}_2 + \kappa_2)u_{y,yy} + (\hat{C} + \lambda_2)\theta_{z,y} - (\hat{\xi}_1 + \kappa_1)\theta_{z,x} = \hat{\rho}\ddot{u}_x \tag{22}$$

$$(\hat{B} + \lambda_1)u_{y,yy} + (\hat{C} + \lambda_2)u_{y,xx} + (\hat{\xi}_2 + \kappa_2)u_{x,xx} - (\hat{\xi}_1 + \kappa_1)u_{x,yy} - (\hat{C} + \lambda_2)\theta_{z,x} - (\hat{\xi}_1 + \kappa_1)\theta_{z,y} = \hat{\rho}\ddot{u}_y \tag{23}$$

$$(\hat{C} + \lambda_2)\left(u_{y,x} - u_{x,y}\right) + (\hat{\xi}_2 + \kappa_2)\left(u_{x,x} + u_{y,y}\right) - 2(\hat{C} + \lambda_2)\theta_z + (\hat{\chi} + \lambda_3)\left(\theta_{z,xx} + \theta_{z,yy}\right) = \hat{J}\ddot{\theta}_z \tag{24}$$

The coefficients λ_i and κ_i appear in the equations of motion (Eqs. (22)–(24)) only when the solid exhibits Form II of chiral, nonreciprocal elasticity, as these moduli vanish when the solid is subjected to only one deformation field, e.g., $u_{i,j}$ or θ_z, while these moduli are non-zero when we act on the solid with multiple deformation fields.

By introducing the force stress tensor τ_{ij} and the couple stress vector m_i, Eqs. (22)–(24) can be written in the form:

$$\begin{aligned} \tau_{xx,x} + \tau_{yx,y} &= \hat{\rho}\ddot{u}_x \\ \tau_{xy,x} + \tau_{yy,y} &= \hat{\rho}\ddot{u}_y \\ m_{x,x} + m_{y,y} + s_z &= \hat{J}\ddot{\theta}_z \end{aligned} \tag{25}$$

where the force stresses τ_{ij} are developed due to the direct displacement-based interactions of the circles, while the couple stresses m_i are developed due to spin-spin interactions of the circles.

In Eq. (25), s_z is an internal body torque/couple that is developed due to applied external forces acting at the external surfaces of the solid material, and thus it is related to the force stresses τ_{ij}, as follows:

$$s_z = \epsilon_{ij}\tau_{ij} = \tau_{xy} - \tau_{yx} \tag{26}$$

where ϵ_{ij} is the 2D Levi-Civita symbol. The internal body torque s_z is defined as in Eq. (26) to satisfy the conservation of the total angular momentum of continua with internal spins (Markovich et al., 2019). It should be noted that the internal body torque s_z is spontaneously developed during the deformation of the chiral solid, and thus it is distinct from any external body torques that would act on the solid.

3.1.3. Constitutive relations

By comparing Eq. (25) with Eqs. (22)–(24), the following constitutive relations are obtained:

$$\begin{Bmatrix} \tau_{xx} \\ \tau_{yy} \\ \tau_{xy} \\ \tau_{yx} \end{Bmatrix} = \begin{bmatrix} \hat{B}+\lambda_1 & 0 & \hat{\xi}_1+\kappa_1 & 0 \\ 0 & \hat{B}+\lambda_1 & 0 & -(\hat{\xi}_1+\kappa_1) \\ \hat{\xi}_2+\kappa_2 & 0 & \hat{C}+\lambda_2 & 0 \\ 0 & -(\hat{\xi}_2+\kappa_2) & 0 & \hat{C}+\lambda_2 \end{bmatrix} \begin{Bmatrix} u_{x,x} \\ u_{y,y} \\ u_{y,x}-\theta_z \\ u_{x,y}+\theta_z \end{Bmatrix} \text{ i.e., } \tau_{ij} = C_{ijkl}(u_{l,k}+\epsilon_{lk}\theta_z) \tag{27}$$

and

$$m_x = (\hat{\chi}+\lambda_3)\theta_{z,x} \& m_y = (\hat{\chi}+\lambda_3)\theta_{z,y} \quad \text{i.e.,} \quad m_i = (\hat{\chi}+\lambda_3)\theta_{z,i} \tag{28}$$

where C_{ijkl} is the fourth-rank elasticity tensor, which is obtained non-symmetric, i.e., $C_{ijkl} \neq C_{klij}$ as shown in Eq. (27). We can write the constitutive law $\tau_{ij} = C_{ijkl}(u_{l,k}+\epsilon_{lk}\theta_z)$ in Eq. (27) in the form $\sigma_\alpha = C_{\alpha\beta}\gamma_\beta$ shown in Eq. (11), as follows:

$$\begin{Bmatrix} \sigma_1 \\ \sigma_2 \\ \sigma_3 \\ \sigma_4 \end{Bmatrix} = \begin{bmatrix} \hat{B}+\lambda_1 & -(\hat{A}+\beta) & 0 & 0 \\ -(\hat{A}-\beta) & \hat{C}+\lambda_2 & 0 & 0 \\ 0 & 0 & \hat{B}+\lambda_1 & \hat{A}+\beta \\ 0 & 0 & \hat{A}-\beta & \hat{C}+\lambda_2 \end{bmatrix} \begin{Bmatrix} \gamma_1 \\ \gamma_2 \\ \gamma_3 \\ \gamma_4 \end{Bmatrix} \textit{ i.e., } \sigma_\alpha = C_{\alpha\beta}\gamma_\beta \tag{29}$$

where $\hat{A} = (\hat{\xi}_1+\hat{\xi}_2+\kappa_1+\kappa_2)/2$ and $\beta = (\hat{\xi}_1-\hat{\xi}_2+\kappa_1-\kappa_2)/2$. The stress components σ_α and the deformations γ_β in Eq. (29) are defined as:

$$\begin{aligned} &\sigma_1 = \tau_{xx}+\tau_{yy}, \sigma_2 = \tau_{yx}-\tau_{xy}, \sigma_3 = \tau_{xx}-\tau_{yy}, \sigma_4 = \tau_{xy}+\tau_{yx} \\ &\gamma_1 = u_{x,x}+u_{y,y}, \gamma_2 = u_{x,y}-u_{y,x}+2\theta_z, \gamma_3 = u_{x,x}-u_{y,y}, \gamma_4 = u_{x,y}+u_{y,x} \end{aligned} \tag{30}$$

It is important to note the difference between the definition of the deformation field γ_2 in Eq. (11) and the one in Eq. (29). In Eq. (11) the 2D solid is assumed to have only translational (i.e., u_x and u_y) degrees of freedom, and thus $\gamma_2 = u_{x,y} - u_{y,x}$ is rotation at the solid's external boundary. On the other hand, as the chiral metamaterial possesses an additional degree of freedom that is a spin field θ_z representing the spin of the rigid circle about its center, the deformation field $\gamma_2 = u_{x,y} - u_{y,x} + 2\theta_z$ is defined as the relative rotation field that is the difference between the rotation at the external boundary of the metamaterial $u_{x,y} - u_{y,x}$ and the internal spin at the circles $2\theta_z$.

The constitutive law in Eq. (29) represents one of the major results of this work, as all subsequent discussions and analysis will utilize this law, and as such we make several remarks here. First, this constitutive law represents an isotropic chiral solid which conserves linear momentum where its stress σ_α is directly proportional to strain γ_β, but which also exhibits chiral, nonreciprocal elasticity. The chiral, nonreciprocal elasticity of the chiral metamaterial is evident in the elasticity tensor $C_{\alpha\beta}$ in Eq. (29) (compare Eq. (29) to Eq. (11)), as demonstrated next.

Second, the elasticity tensor $C_{\alpha\beta}$ in Eq. (29) is chiral as it breaks the reflection–rotation symmetry by having non-zero chiral moduli $\hat{A}$ and β. These moduli enable the chiral metamaterial to develop (1) dilation due to rotation of its external boundary or spinning of its rigid circles, (2) rotation at the external boundary or spin at the rigid circles due to dilation, (3) shear deformations due to axial strains, and (4) axial strains due to shear deformations.

Third, the elasticity tensor $C_{\alpha\beta}$ reveals directional nonreciprocity, as all of its elastic moduli are modulated depending on the direction of the applied deformation/stress (recall Fig. 1(a) and the $\pm$ superscripts from Eq. (11)). The form of the elasticity tensor does not change, though the values of all elastic moduli change by the spatial inversion of the applied deformation/stress.

Fourth, the elasticity tensor $C_{\alpha\beta}$ can be decomposed into *symmetric* and *skew-symmetric* elasticity tensors, with the skew-symmetric tensor depending on the chiral modulus β, revealing Form I of chiral nonreciprocity, i.e., where the chiral coupling between two different deformation modes (e.g., dilation and rotation) is nonreciprocal (recall Figs. 1(b) and 1(c)). The elasticity tensor is symmetric when $\beta = 0$, and thus the chiral modulus β is what enables Form I of chiral nonreciprocity of the chiral metamaterial.

Fifth, the elasticity tensor also models Form II of chiral nonreciprocity, as the elastic moduli λ_1 and λ_2 appear only when the solid is subjected to coupled deformation fields (recall Fig. 1(d) and Eq. (11)). The elastic moduli λ_1 and λ_2 represent the modulation of, respectively, the elastic bulk modulus $\hat{B}$ and the elastic torsional modulus $\hat{C}$ by deforming the chiral metamaterial with coupled deformation fields.

Remark 2. Because the modulation of the elastic moduli of $C_{\alpha\beta}$ depends on the directions of and the coupling between the different deformation fields, there may be a set of deformations at which the elastic moduli λ_1, λ_2, and β are zero, and thus the elasticity tensor becomes reciprocal, but chiral (see Table A.2 of Appendix A).

3.2. Numerical demonstration of chiral, nonreciprocal elasticity

Having analytically established the chiral, nonreciprocal elastic constitutive law in Eq. (29), we now demonstrate the chiral, nonreciprocal constitutive behavior of the chiral metamaterial using finite element simulations when it undergoes deformations that satisfy the conditions in Remark 1 above. While we could deform the chiral metamaterial in arbitrary ways resulting in highly complex deformation fields and complicated field equations, which then should be solved for the kinematical degrees of freedom u_x, u_y, and θ_z, we instead demonstrate the chiral, nonreciprocal elasticity by subjecting the chiral metamaterial to uniform deformation fields that are simple yet demonstrate the constitutive law in Eq. (29). As such, we consider here and for the remainder of the paper the chiral metamaterial shown in Fig. 2(a) under the various deformation fields shown in Fig. 4, where it can be deformed by uniform dilation $\gamma_1 = u_{x,x} + u_{y,y}$ (Fig. 4(a)), uniform rotation $\gamma_2 = u_{x,y} - u_{y,x}$ (Fig. 4(b)), and uniform spin $\gamma_2 = 2\theta_z$ (Fig. 4(c)). For each of these deformations, to have the chiral metamaterial exhibits only one deformation field (e.g., in Fig. 4(a) the chiral metamaterial exhibits dilation only, where all other deformations are zero), the deformations in Figs. 4(a) and 4(b) are carried out such that the rigid circles can translate but not spin, while in Fig. 4(c), the circles only spin, but do not translate. In addition, to avoid rigid body rotations, the rotation $(u_{x,y} - u_{y,x})$ in Fig. 4(b) is performed at zero spin $\theta_z = 0$, while the spin θ_z in Fig. 4(c) is performed at zero rotation $u_{x,y} - u_{y,x} = 0$.

Remark 3. When the chiral metamaterial is deformed under the deformations shown in Figs. 4(a)-4(c), the torsional stress σ_2 is non-zero, meaning that the stress tensor is non-symmetric, i.e., $\tau_{ij} \neq \tau_{ji}$, and thus the angular momentum is not conserved. To conserve angular momentum, the chiral metamaterial should be deformed such that $\sigma_2 = 0$, which can be done by having both γ_1 and γ_2 non-zero (see Eq. (29)), e.g., dilation is carried out while the circles are free to spin. See Section 4.3 for more details.

Remark 4. In addition to the chiral, nonreciprocal elasticity manifested in the force-stress tensor in Eq. (29), the chiral metamaterial also reveals chiral, nonreciprocal couple stress fields m_i (see Eq. (28)). In Eq. (28), the elastic modulus $\hat{\chi}$ is modulated depending on the direction of the applied deformation as well as by coupling the spin gradient $\theta_{z,i}$ with any other deformation field, e.g., dilation, where the modulus λ_3 is the change in $\hat{\chi}$ due to coupling. As the focus of this study is to reveal only the chiral, nonreciprocal elastic behaviors manifested in the constitutive law in Eq. (29), we eliminate couple stress effects by considering uniform spin field (i.e., $\theta_{z,i} = 0$), and therefore the couple stress m_i is zero for the different deformations shown in Fig. 4. Chiral, nonreciprocal couple stress effects will be considered in future work.

To demonstrate directional nonreciprocity via the modulation of the elastic moduli of the elasticity tensor $C_{\alpha\beta}$ in Eq. (29) by the spatial inversion of the deformation, we performed finite element simulations of the chiral metamaterial shown in Fig. 2(a) when it is deformed by a single deformation field (i.e., with the resulting nonreciprocal stress–strain response shown in Figs. 4(d)-4(f)) (see Appendix A for more details on the finite element simulations). Specifically, Fig. 4(d) demonstrates the mechanical response of the chiral metamaterial under dilation γ_1 (Fig. 4(a)), where the finite element analysis was initiated from a zero stress state, i.e. $\sigma_\alpha^0 = 0$ where the superscript (0) indicates an initial stress, and where tensile dilation $\gamma_1 = +0.0125$ and compressive dilation $\gamma_1 = -0.0125$ were applied. The non-zero stresses developed in the chiral metamaterial were numerically determined as $\sigma_1 = 44.88$ MPa and $\sigma_2 = -25.3$ MPa for the tensile dilation, while these stresses were obtained as $\sigma_1 = -21.45$ MPa and $\sigma_2 = 10.55$ MPa for the compressive dilation. It should be noted that, because of the chirality, in addition to the dilatational stress σ_1, the torsional stress σ_2 is developed, and thus according to Eq. (29), two elastic moduli emerge where $\hat{A} - \beta$ is the modulus of the chiral coupling. By calculating the slope of the stress–strain curves, the elastic moduli $\hat{B} = \sigma_1/\gamma_1$ and $\hat{A} - \beta = \sigma_2/\gamma_1$ were determined. The chiral metamaterial showed higher stiffness in tension than in compression, and thus the bulk modulus $\hat{B}$ and the chiral modulus $\hat{A} - \beta$ were obtained by $\hat{B} = 3592$ MPa and $\hat{A} - \beta = 2025$ MPa for tensile dilation, and $\hat{B} = 1716$ MPa and $\hat{A} - \beta = 843.7$ MPa for compressive dilation (Fig. 4(d)). Thus, the bulk modulus $\hat{B}$ and the chiral modulus $\hat{A} - \beta$ are both modulated by the spatial inversion of the applied dilation. This contrast in the elastic response of the chiral metamaterial due to the change of the direction of the applied dilation is dependent on the mechanism of the chiral element deformation shown in Fig. 3, and specifically, how the ligaments of the chiral structure are attached to or detached from the rigid circles during the deformation. For the applied deformations in Fig. 4, in one direction, the ligaments are detached completely from the rigid circles resulting in a low stiffness, whereas in the opposite direction, the ligaments are pressed against the circles such that the curved ends of the ligaments come into full contact with the circles, resulting in a high stiffness. In general, and as demonstrated in Figs. 4(d)-4(f), the chiral metamaterial modulates its elastic moduli through the spatial inversion of an applied dilation, rotation, or spin.

In addition to the directional nonreciprocity, we also demonstrate asymmetric elasticity (Form I of chiral, nonreciprocal elasticity) of the chiral metamaterial through finite element simulations. Specifically, in Figs. 4(d)-4(f), we compare the elastic moduli of the chiral coupling $\hat{A} \pm \beta$ obtained by deforming the chiral metamaterial independently with dilation (Fig. 4(a)), rotation (Fig. 4(b)), and spin (Fig. 4(c)). It follows that the dilation–rotation coupling and the dilation-spin coupling are not reciprocal, as the torsional stress σ_2 developed due to dilation γ_1 in Fig. 4(d) is not equivalent to the dilatational stress σ_1 developed due to rotation or spin γ_2 in Figs. 4(e) or 4(f). For example, the elastic modulus of the dilation–rotation coupling was obtained by $\hat{A} - \beta = 843.7$ MPa due to compressive dilation, while it was obtained by $\hat{A} + \beta = 2018$ MPa due to counterclockwise rotation (see Figs. 4(d) and 4(e)). This contrast in the coupling moduli gives the chiral modulus β non-zero, such that $\hat{A} = 1431$ MPa and $\beta = 587.2$ MPa, and thus reveals asymmetric elasticity of the chiral metamaterial. We emphasize that the values of the elastic moduli $\hat{A}$ and β still may change by the spatial inversion of either one of the coupled deformation fields, and thus there is a set of deformations at which the chiral solid exhibits symmetric elasticity, where in this case β becomes zero (see Appendix A). In general, the asymmetric elastic response

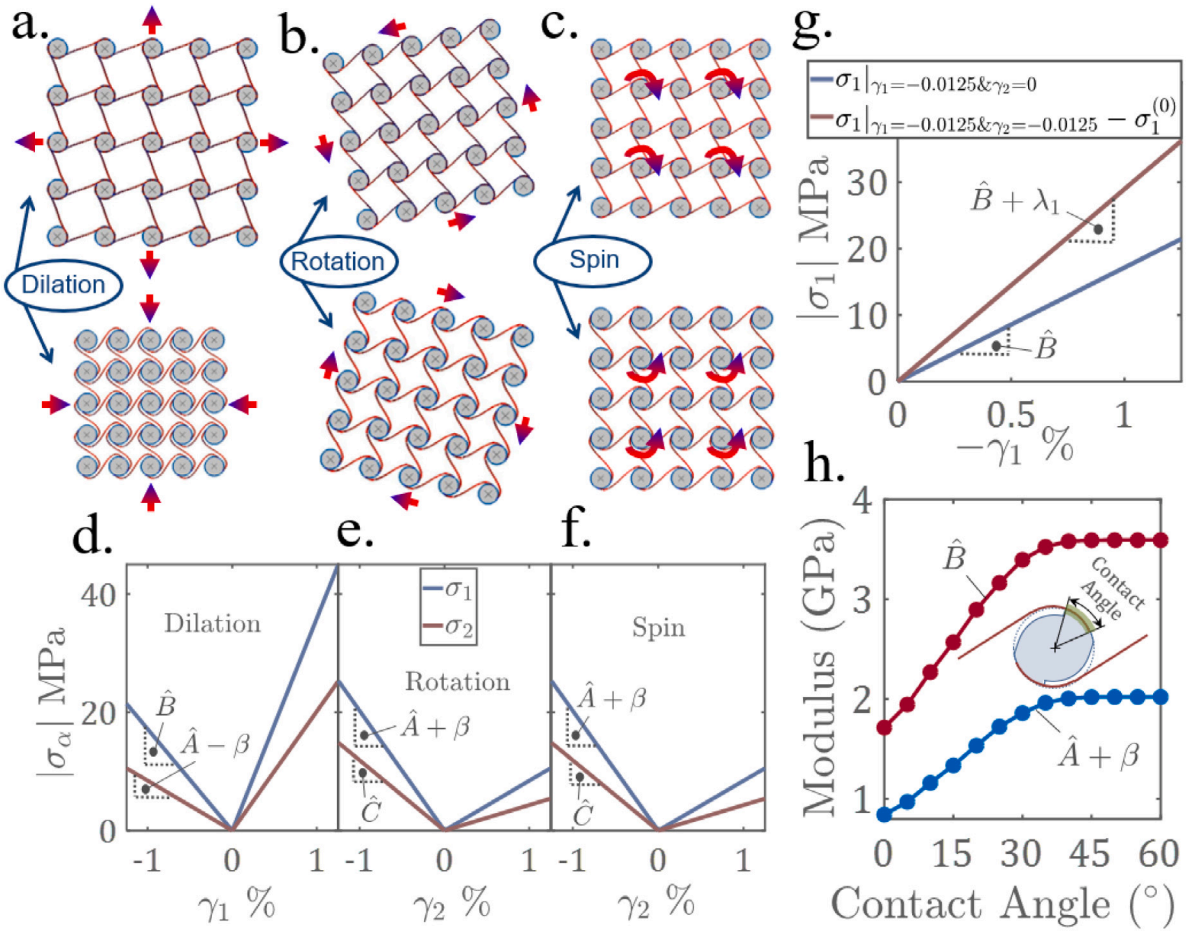

Fig. 4. Chiral, nonreciprocal elasticity of the chiral metamaterial. (a-c) Examples of elastic deformations that enable chiral, nonreciprocal elasticity of the chiral metamaterial. These deformations were obtained through finite element simulations using ABAQUS (see Appendix A for more details), where the chiral metamaterial was deformed by (a) dilation $\gamma_1 = u_{x,x} + u_{y,y} = \pm 0.0125$ where $u_{x,x} = u_{y,y}$, (b) rotation $\gamma_2 = u_{x,y} - u_{y,x} = \pm 0.0125$ where $u_{x,y} = -u_{y,x}$, and (c) spin $\gamma_2 = 2\theta_z = \pm 0.0125$. The deformations in (a) and (b) were carried out such that the rigid circles can translate but not spin, while in (c), the circles only spin, but do not translate. To avoid rigid body rotations, the rotation $(u_{x,y} - u_{y,x})$ in (b) was performed at zero spin $\theta_z = 0$, while the spin θ_z in (c) was performed at zero rotation $u_{x,y} - u_{y,x} = 0$. (d–g) Elastic stress–strain curves of the chiral metamaterial determined by finite element simulations. (d-f) Directional and Form I of chiral, nonreciprocal elasticity. The chiral metamaterial was deformed by a single deformation field, i.e., (d) dilation $\gamma_1 = u_{x,x} + u_{y,y} = \pm 0.0125$, where $u_{x,x} = u_{y,y}$, (e) rotation $\gamma_2 = u_{x,y} - u_{y,x} = \pm 0.0125$, where $u_{x,y} = -u_{y,x}$, and (f) spin $\gamma_2 = 2\theta_z = \pm 0.0125$. In (d-f), the elastic moduli in Eq. (29) were determined by calculating the slope of the stress–strain curve, which were obtained depending on the direction of the applied deformation. (g) Form II of chiral, nonreciprocal elasticity. Comparison of the bulk modulus obtained when deforming the chiral metamaterial by only compressive dilation $\sigma_1|_{\gamma_1=-0.0125\ \&\ \gamma_2=0} = \hat{B}\gamma_1$ to the bulk modulus obtained by deforming the chiral metamaterial by counterclockwise rotation and compressive dilation $\sigma_1|_{\gamma_1=-0.0125\ \&\ \gamma_2=-0.0125} - \sigma_1^{(0)} = (\hat{B}+\lambda_1)\gamma_1$, where $\sigma_1^{(0)} = \sigma_1|_{\gamma_1=0\ \&\ \gamma_2=-0.0125}$ is an initial dilatational stress developed by the introduction of the rotation. The modulus $\hat{B}$ changes to $\hat{B}+\lambda_1$ after the introduction of rotation. (h) The variations of the bulk modulus $\hat{B}$ and the chiral coupling modulus $\hat{A}+\beta$ as functions of the area of contact established between the ligaments and the rigid circles. These results were determined based on ABAQUS finite element simulations of the chiral structure shown in Fig. 2(c), but different circle profiles were used for the different contact angles.

(Form I of chiral, nonreciprocal elasticity) of the chiral metamaterial arises when the contact state is different between the two deformation modes, while it is suppressed when the contact state is the same between the two deformation modes.

To demonstrate Form II of chiral, nonreciprocal elasticity, where the chiral metamaterial can also modulate its elastic moduli by deforming it with coupled deformation fields, we show in Fig. 4(g) the mechanical response of the chiral metamaterial under the dilation–rotation coupling—specifically, we compare (1) the response when the chiral metamaterial is deformed by compressive dilation alone, i.e., $\gamma_1 = -0.0125$ & $\gamma_2 = 0$ to (2) the response when it is deformed by counterclockwise rotation and compressive dilation, i.e., $\gamma_1 = -0.0125$ & $\gamma_2 = -0.0125$. The bulk modulus $\hat{B}$ when the chiral metamaterial was deformed by dilation alone was determined by $\hat{B} = \sigma_1/\gamma_1 = 1716$ MPa, while because the chiral metamaterial maintains coupling between rotation and dilation, the bulk modulus $\hat{B}$ is modulated by the introduction of the rotation $\gamma_2 = -0.0125$, where a different bulk modulus value was determined by $\hat{B} + \lambda_1 = (\sigma_1 - \sigma_1^{(0)})/\gamma_1 = 2890$ MPa, where $\sigma_1^{(0)}$ is the initial dilatational stress developed by the introduction of the rotation. By comparing these two values of the bulk modulus, the elastic modulus λ_1 was calculated by $\lambda_1 = 1174$ MPa, which indicates that the chiral metamaterial can modulate its elastic moduli if coupled deformation fields are simultaneously applied.

We also note that, for the considered chiral metamaterial, the mechanisms of enabling the various forms of chiral nonreciprocity shown in Fig. 1 are not independent from one another. These mechanisms are rather related and unified by the geometrical and material characteristics of the chiral structure, as the chiral metamaterial cannot exhibit one form of chiral nonreciprocity without the others. For instance, the directional nonreciprocity is eliminated along with the elastic moduli λ_1, λ_2 and β, which enable Form I and Form II of chiral, nonreciprocal elasticity of the solid, and thus the entire chiral, nonreciprocal elastic effect is eliminated, if the isotropic metamaterial is either achiral (i.e., $\alpha_0 = 0$) or reciprocal (i.e., $\theta_0 = 0$). Therefore, the attainment of chirality and nonreciprocity enables chiral, nonreciprocal elasticity of the chiral metamaterial, with all forms of chiral nonreciprocity emerging simultaneously.

It is important to note that the stiffness of the chiral metamaterial depends on the area of the contact established between the curved ends of the ligaments and the rigid circles, such that the minimum stiffness value is obtained when the ligaments are detached completely from the circles and thus no contact is developed, while the maximum value of the stiffness is obtained when the curved ends of the ligaments come into full contact with the circles. The area of the contact that can be established between the ligaments and the circles depends on the profile of the curved end of the ligament and the profile of the rigid circle. By changing either one of the two profiles, the area of the contact changes, resulting in a different stiffness of the chiral metamaterial. For instance, we present in Fig. 4(h) the slope of the stress–strain curves of the chiral metamaterial under tensile dilation only ($+\gamma_1$) (for the bulk modulus $\hat{B}$) or counterclockwise rotation only ($-\gamma_2$) (for the chiral modulus $\hat{A}+\beta$) for different profiles of the rigid circle. It is clear that the elastic moduli of the chiral metamaterial increase due to an increase in the area of contact established between the ligament and the circle.

Before moving forward, it is also important to discuss other implications of the non-reciprocal nature of the elasticity tensor developed in Eq. (29). As just discussed, the values of the elastic moduli vary depending upon what deformation or combination of deformations are imposed. In one sense, this implies that the chiral metamaterial is a type of smart material, which can adjust its mechanical response depending on the type of loading it is subject to. On the other hand as previously discussed, this adds complication in using the constitutive model in Eq. (29), due to the fact that it must be known a priori what deformations are going to be applied to the chiral metamaterial in order to have an accurate model for its resulting mechanical response.

Remark 5. Whereas the constitutive response can be linear elastic as shown in Fig. 4, the chiral metamaterial being nonreciprocal implies that it is a nonlinear material system that does not always satisfy the superposition principle, as when we apply equal and opposite deformations on the chiral metamaterial, the net force is not zero, i.e., $F(u)+F(-u) = F(u-(-u)) \neq 0$. Therefore, this system, like other recent examples of asymmetric elasticity (Scheibner et al., 2020; Chen et al., 2021b; Brandenbourger et al., 2022), violates Maxwell–Betti reciprocity.

4. Mechanical activity of the 2D chiral metamaterial

Above, we established the constitutive model for the chiral metamaterial shown in Fig. 2 via Eq. (29), and also demonstrated, via finite element simulations, that its mechanical response is non-symmetric and nonreciprocal (Fig. 4), where previous works have demonstrated that if a linear, elastic solid has asymmetric elasticity, it enables mechanical activity in which the solid can interact with the surrounding with mechanical work (Chen et al., 2021b; Scheibner et al., 2020). Here, we first theoretically demonstrate the mechanical activity of the chiral metamaterial within the context of the developed chiral nonreciprocal elastic constitutive law (Eq. (29)) - specifically, we demonstrate that our chiral metamaterial that is made of passive chiral elements can break energy conservation, and thus it can interact with the surrounding with mechanical work when it is used in specific cycles of quasistatic deformations. Next, we demonstrate through numerical finite element simulations the practical implementation of these deformation cycles, while elucidating the specific conditions needed for the chiral metamaterial to exhibit linear, chiral nonreciprocal elastic behavior throughout the deformation cycle and thus to reveal mechanical activity.

4.1. Mechanical activity: Theoretical demonstration

We first develop a thermodynamic framework of energy balance and energy conservation of chiral, nonreciprocal elastic solids, based on which we demonstrate theoretically within the context of the developed analytical model that the described chiral, nonreciprocal elasticity enables *static thermodynamic non-equilibrium* (violation of thermodynamic equilibrium without dynamics) and thus enables *mechanical activity* of elastic solids at zero-frequency.

4.1.1. Thermodynamics: energy balance

The energy balance of a system is the concern of the first law of thermodynamics, which states that the net energy transfer to (or from) the system from (or to) its surroundings in the form of heat δQ or work δW is equal to the net change in the total energy of the system $\mathrm{d}U$, i.e., $\mathrm{d}U = \delta Q + \delta W$. The second law of thermodynamics, on the other hand, defines the internal entropy change $\mathrm{d}S$ of the system by $\mathrm{d}S = \delta Q/T$ as it undergoes *reversible thermodynamic processes*, or by $\mathrm{d}S \geq \delta Q/T$ when it undergoes *irreversible thermodynamic processes*, where T is the absolute temperature of the system surroundings. Given this thermodynamic standpoint of physical systems, and as elasticity describes *reversible* material deformations, we can establish the condition of energy balance in elastic solids by substituting the first law into the second law of thermodynamics, as follows (assuming isothermal processes, i.e., $\mathrm{d}T = 0$):

$$\delta W = \mathrm{d}\psi \tag{31}$$

where $\psi = U - TS$ is the Helmholtz free energy, which expresses the maximum internal capacity of a system undergoing an isothermal process to do (receive) work on (from) its surroundings. This law states that in the absence of irreversible interactions with the surroundings, the work δW needed to drive an elastic solid through an isothermal deformation process between two states is equal to the net change in the solid's internal free energy $\mathrm{d}\psi$ between the two states. The violation of the energy balance in Eq. (31) indicates an *inelastic* solid that exhibits irreversible deformations due to internal energy sources that result in energy gain or loss (i.e., non-conservation of energy). However, inelastic solids are outside the scope of the present study, as the developed chiral, nonreciprocal elasticity defines a class of elastic solids that do not contain energy sources, and thus always satisfy the energy balance in Eq. (31) when undergoing reversible interactions with the surroundings.

4.1.2. Thermodynamics: energy conservation

Having established the energy balance of chiral, nonreciprocal elastic solids, we examine here the conservation of energy as the chiral, nonreciprocal elastic solid undergoes a closed cycle of a sequence of reversible deformations, in each of which the energy balance law in Eq. (31) must be satisfied.

There are two different notations for the differential used in Eq. (31), i.e., 'd' and 'δ', where 'd' defines a differential whose integral does not depend on the path of the thermodynamic (or deformation) process, while 'δ' is a differential whose integral is path dependent. Therefore, the internal, free energy ψ is a state function whose integral over a deformation cycle Ω depends only on the initial and final states of the solid in the cycle, i.e., $\oint_{\partial\Omega} \mathrm{d}\psi = \psi_{\text{final}} - \psi_{\text{initial}}$, and thus the net change in the internal, free energy of the solid through a *closed* deformation cycle is zero, i.e., $\oint_{\partial\Omega} \mathrm{d}\psi = 0$, as the state of the solid at the beginning and the end of the cycle is the same $\psi_{\text{final}} = \psi_{\text{initial}}$. The work δW however is not a state variable, as its integral over a deformation cycle gives a *cumulative work* $\oint_{\partial\Omega} \delta W$ that depends on the path of the deformation cycle. If the cumulative work used to drive the solid through the deformation cycle equals the net change in the solid's internal, free energy through the cycle (i.e., $\oint_{\partial\Omega} \delta W = \oint_{\partial\Omega} \mathrm{d}\psi$), the energy of deforming the solid through the cycle is conserved, and it is not conserved otherwise. Therefore, the difference between the cumulative work and the net change in the internal energy of the solid, i.e., $W = \oint_{\partial\Omega} \delta W - \oint_{\partial\Omega} \mathrm{d}\psi$, is a *mechanical work* that can be obtained by deforming the solid through a deformation cycle.

The conventional route to break energy conservation of a solid material system (i.e., $\oint \delta W - \oint \mathrm{d}\psi \neq 0$) depends on using the solid through a cycle of irreversible deformation processes, in which the solid does not satisfy the energy balance in Eq. (31), and this requires the solid be made with an internal, microscopic energy source that would supply or consume energy as the solid is used through the deformation cycle. Unlike this route, in this study, we demonstrate a different route of breaking energy conservation for a class of elastic solids that always satisfy the energy balance in Eq. (31), and thus these solids must not be connected to energy sources. At the absence of energy sources, the cumulative work W of deforming an elastic solid through a closed deformation cycle can be non-zero if the solid exhibits non-symmetric elastic response, or – in general – modulation of its elastic properties during the deformation cycle. Consider for instance an elastic solid whose stiffness is $k_{\alpha\beta}$ undergoing a closed deformation cycle of displacement-controlled deformations u_α. The cumulative work developed by deforming the elastic solid through the closed deformation cycle can be then determined by $W = \oint \delta W = \oint_0^{u_\alpha} (k_{\alpha\beta} u_\beta) \delta u_\alpha = (k_{\alpha\beta} - k_{\beta\alpha}) u_\beta u_\alpha$, which is non-zero as long as $k_{\alpha\beta} \neq k_{\beta\alpha}$. Thus, energy conservation can be broken by enabling the elastic solid to exhibit a non-symmetric response through spontaneous modulation of the stiffness as the solid is deformed, which can be achieved by means that does not require the use of active components that consume energy (i.e., without energy sources). Enabled by its chiral, nonreciprocal elasticity, the stiffness/elastic properties of the considered chiral metamaterial in Fig. 2 can change depending on the direction and mode of the applied deformation (see Fig. 4), and thus the chiral metamaterial can break energy conservation, and it can interact with the surrounding with mechanical work without using energy sources. Based on the chiral, nonreciprocal constitutive model of the chiral metamaterial in Eqs. (27)–(29), next we analytically demonstrate the mechanical work that can be obtained by deforming the chiral metamaterial through a closed deformation cycle.

4.1.3. Energy conservation of the chiral metamaterial

For the considered chiral metamaterial in Fig. 2, the work δW needed to deform it through a quasistatic deformation process satisfying the energy balance in Eq. (31) takes the form $\delta W = \int_V \delta w dV$, where δw is the first variation of the internal energy per unit volume V of the chiral solid. The variation δw is an infinitesimal change in the solid's internal energy, which can be determined based on the Hamilton's principle and after considering the equations of motion in Eq. (25), as follows:

$$\delta w = \tau_{ji} \delta u_{i,j} + \hat{M} \delta \theta_z \tag{32}$$

where $\hat{M} = -m_{i,i} - s_z$. By substituting Eqs. (27) and (28) into Eq. (32), and based on the sum rule of derivatives, δw can be written as the sum of the variation of potential energy density δw_p and variations that depend on chiral nonreciprocity (cn) and thus cannot be obtained from potential energy δw_{cn}, as follows:

$$\begin{aligned}
&\delta w = \delta w_p + \delta w_{cn} \text{ i.e.,} \\
&\delta w_p = \tfrac{1}{2}\delta \Big[\hat{B} \left(u_{x,x}^2 + u_{y,y}^2 \right) + \hat{C} \left(u_{x,y}^2 + u_{y,x}^2 \right) + 2\hat{C}\theta_z^2 + 2\hat{C}\theta_z \left(u_{x,y} - u_{y,x} \right) - \left(\hat{\xi}_1 + \hat{\xi}_2 \right) \theta_z \left(u_{x,x} + u_{y,y} \right) \\
&\qquad + \left(\hat{\xi}_1 + \hat{\xi}_2 \right) \left(u_{y,x} u_{x,x} - u_{y,y} u_{x,y} \right) + \hat{\chi} \left(\theta_{z,x}^2 + \theta_{z,y}^2 \right) \Big] \\
&\delta w_{cn} = \tfrac{1}{2} \left(\hat{\xi}_2 - \hat{\xi}_1 \right) \left[\theta_z \delta \left(u_{x,x} + u_{y,y} \right) - \left(u_{x,x} + u_{y,y} \right) \delta \theta_z - u_{y,x} \delta u_{x,x} - u_{y,y} \delta u_{x,y} + u_{x,x} \delta u_{y,x} + u_{x,y} \delta u_{y,y} \right] \\
&\quad + \lambda_1 \left(u_{x,x} \delta u_{x,x} + u_{y,y} \delta u_{y,y} \right) + \lambda_2 \left[u_{y,x} \delta u_{y,x} + u_{x,y} \delta u_{x,y} + \theta_z \delta \left(u_{x,y} - u_{y,x} \right) + \left(u_{x,y} - u_{y,x} \right) \delta \theta_z + 2\theta_z \delta \theta_z \right] \\
&- \lambda_3 \left(\theta_{z,xx} + \theta_{z,yy} \right) \delta \theta_z + \kappa_1 \left[u_{y,x} \delta u_{x,x} - u_{x,y} \delta u_{y,y} - \theta_z \delta \left(u_{x,x} + u_{y,y} \right) \right] + \kappa_2 \left[u_{x,x} \delta u_{y,x} - u_{y,y} \delta u_{x,y} - \left(u_{x,x} + u_{y,y} \right) \delta \theta_z \right]
\end{aligned} \tag{33}$$

The variation of the potential energy δw_p is obtainable from a quadratic, free energy function, while the variations δw_{cn} cannot be expressed as the variation of potential energy and thus cannot be obtained assuming a free energy function. The appearance of the variations δw_{cn} in the energy balance of the chiral metamaterial is contingent on the metamaterial being chiral, nonreciprocal elastic. These variations enable mechanical activity of the chiral metamaterial when it is used through closed cycles of quasistatic deformations, as the chiral metamaterial can act on a mechanical component connected to it with mechanical work as it is deformed through the cycle. For a closed deformation cycle, the change in the internal energy is zero, i.e., $\mathrm{d}\psi = 0$, and thus the mechanical work W that can be obtained by deforming the chiral metamaterial through a closed deformation cycle equals the cumulative work, which can be determined by integrating the differential of the internal energy density δw over the closed loop of the deformation space Ω (i.e., $W = \oint_{\partial\Omega} \delta w = \oint_{\partial\Omega} \delta w_p + \oint_{\partial\Omega} \delta w_{cn}$), which gives according to Green's theorem:

$$\begin{aligned} W = \oint_{\Omega} \big[&\left(\hat{\xi}_1 - \hat{\xi}_2\right) \left(\delta u_{x,x}\delta u_{y,x} + \delta u_{x,y}\delta u_{y,y} - \delta\left(u_{x,x} + u_{y,y}\right)\delta\theta_z\right) + \lambda_1 \left(u_{x,x}\delta u_{x,x} + u_{y,y}\delta u_{y,y}\right) \\ &+\lambda_2 \left(u_{y,x}\delta u_{y,x} + u_{x,y}\delta u_{x,y} + \theta_z\delta\left(u_{x,y} - u_{y,x}\right) + \left(u_{x,y} - u_{y,x}\right)\delta\theta_z + 2\theta_z\delta\theta_z\right) - \lambda_3 \left(\theta_{z,xx} + \theta_{z,yy}\right)\delta\theta_z \\ &+\kappa_1 \left(u_{y,x}\delta u_{x,x} - u_{x,y}\delta u_{y,y} - \theta_z\delta\left(u_{x,x} + u_{y,y}\right)\right) + \kappa_2 \left(u_{x,x}\delta u_{y,x} - u_{y,y}\delta u_{x,y} - \left(u_{x,x} + u_{y,y}\right)\delta\theta_z\right)\big] \end{aligned} \tag{34}$$

where W is the cumulative work per unit volume over the deformation cycle of the chiral metamaterial. Utilizing the kinematical variables defined in Eq. (30), the cumulative work W can be written, as follows:

$$W = \oint_{\Omega} \left[\beta \left(\delta\gamma_2\delta\gamma_1 + \delta\gamma_3\delta\gamma_4\right) + \tfrac{1}{2}\lambda_1 \left(\gamma_1\delta\gamma_1 + \gamma_3\delta\gamma_3\right) + \tfrac{1}{2}\lambda_2 \left(\gamma_2\delta\gamma_2 + \gamma_4\delta\gamma_4\right) - \lambda_3 \left(\theta_{z,xx} + \theta_{z,yy}\right)\delta\theta_z\right] \tag{35}$$

It follows from Eqs. (34) and (35) that the energy of the chiral, nonreciprocal elastic metamaterial is not fully conserved, and thus it can act as a source of mechanical work. The emergence of the mechanical work is contingent on (1) the chiral, nonreciprocal elasticity of the solid metamaterial, as the cumulative work W in Eq. (35) depends on the elastic moduli of chiral, nonreciprocity β, λ_1, λ_2, and λ_3, while it is zero when the solid is either achiral or reciprocal elastic. The contact state between the ligaments and the rigid circles may change as the chiral metamaterial is deformed through the deformation cycle, such that the ligaments may be detached from the rigid circles in one or more deformation processes, while in the other deformation processes contact may be established between the ligaments and the circles. This results in chiral nonreciprocity and modulation of the stiffness of the chiral metamaterial through the deformation cycle, and thus mechanical work can be developed. The first term of the cumulative work W in Eq. (35) is developed due to asymmetric elasticity enabled by Form I of the chiral nonreciprocity, while the other terms of W are developed due to Form II of the chiral nonreciprocity. It should be noted that, while it is clear that the form of the first term of W does not express a variation of potential energy, the other three terms of W also do not express variation of potential energy because the elastic moduli λ_1, λ_2, and λ_3 are developed only when the solid is deformed by two coupled deformation fields.

The emergence of the mechanical work is also contingent on (2) using the solid metamaterial through *linear elastic* deformation cycles of coupled deformation fields, as non-zero cumulative work is guaranteed when the elastic moduli of chiral, nonreciprocity β, λ_1, λ_2, and λ_3 are non-zero and constants through the deformation cycle. With these elastic moduli being constants, meaning that the chiral metamaterial must be used in a linear elastic deformation cycle, the cumulative work in Eq. (35) is trivial zero if and only if the moduli β, λ_1, λ_2, and λ_3 are zero. It is therefore important to note that, in complex deformation cycles, in which the chiral metamaterial is deformed by coupled deformation fields, during a deformation process, the chiral structure may undergo a transition between a state where the ligaments are detached from the circles (no contact) and a state where the ligaments come into contact with the circles, resulting in a nonlinear mechanical response during this deformation process, as a manifestation of the nonreciprocity of the chiral metamaterial. Therefore, it is important to maintain the contact state constant through each deformation process of the deformation cycle, as this gives the mechanical response of the chiral metamaterial linear elastic through the cycle, and thus mechanical work can be developed.

It also follows from Eq. (35) that the cumulative work depends on the deformation path, in which the chiral metamaterial should be deformed by a sequence of coupled deformation fields. The chiral metamaterial achieves different forms of chiral coupling including dilation–rotation/spin coupling ($\gamma_1 \Leftrightarrow \gamma_2$) and dilation–shear coupling ($\gamma_3 \Leftrightarrow \gamma_4$), and thus it can develop mechanical work W when it is used through closed cycles that achieve such couplings (see Appendix B for calculations of the cumulative work). The chiral metamaterial can also develop mechanical work by achieving internal gradients of spin $\theta_{z,i}$ and nonreciprocal internal couple stress fields $\lambda_3\theta_{z,i}$, as shown in the last term of Eq. (35). As mentioned in Remark 4, in this study, we focus on elastic behaviors and mechanical activity due to the nonreciprocal force stress fields manifested in the constitutive law in Eq. (29), while the cumulative work due to nonreciprocal couple stress fields (the last term of Eq. (35)) will be considered in a future study.

4.2. Mechanical activity: Practical demonstration

A solid whose elastic response is linear and non-symmetric can interact with the surrounding with mechanical work (Scheibner et al., 2020). While the chiral metamaterial proposed in this work is made from passive elements, and exhibits asymmetric elasticity without being connected to external energy sources, which is in contrast to previous works (Scheibner et al., 2020; Chen et al., 2021b), the theoretical investigation of its mechanical activity above indicates that it can be active when used in a closed deformation cycle of a specific sequence of deformations that enables it to exhibit linear, chiral nonreciprocal elastic behavior. We now discuss how this can be achieved practically using finite element simulations.

Specifically, we demonstrate in Fig. 5 the mechanical activity of our chiral metamaterial by determining the energy gain/loss (i.e., cumulative work W) when it undergoes a quasistatic deformation cycle of coupled dilation and rotation ($\lambda_1 \Leftrightarrow \lambda_2$), where the structural configuration is the same at the beginning and the end of the cycle. We considered a chiral metamaterial that is formed by 4×4 chiral elements (Fig. 2(a)) with a chiral angle $\alpha_0 = 30°$ and lattice length $a = 20$ mm, where the circles are rigid

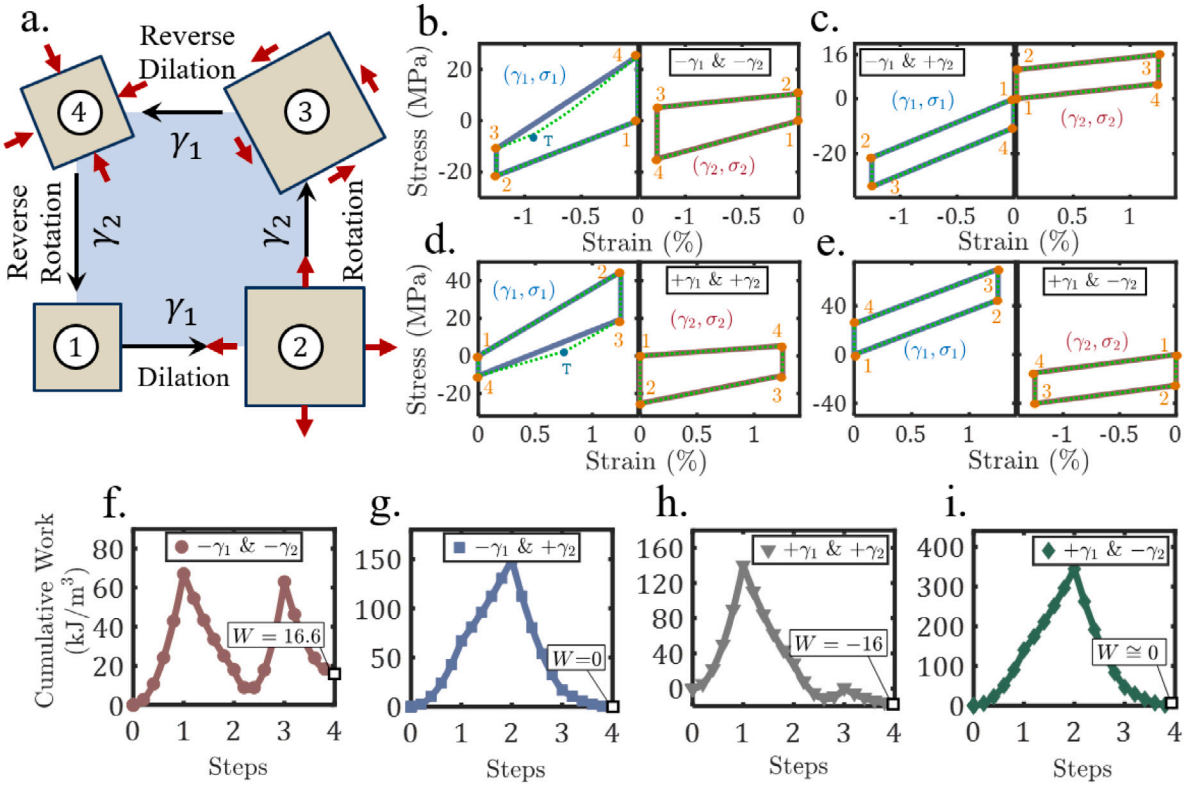

Fig. 5. Mechanical activity of the chiral metamaterial used in linear quasistatic deformation cycles. (a) Representation of a strain-controlled, quasistatic deformation cycle of a sequence of dilation γ_1 and rotation γ_2. (b–e) The variations of the dilatational stress σ_1 and the torsional stress σ_2 versus the applied strain through the deformation cycle. The stresses were determined using ABAQUS finite element simulations of the chiral metamaterial when deformed through the cycle by (b) $\gamma_1 = -0.0125$ and $\gamma_2 = -0.0125$, (c) $\gamma_1 = -0.0125$ and $\gamma_2 = +0.0125$, (d) $\gamma_1 = +0.0125$ and $\gamma_2 = +0.0125$, and (e) $\gamma_1 = +0.0125$ and $\gamma_2 = -0.0125$. During Process $3 \rightarrow 4$, the chiral metamaterial may undergo a transition (as indicated by the letter 'T') from (or to) no contact to (or from) full contact between the ligaments and the circles, resulting in the nonlinear mechanical response shown by the dotted curves. To maintain linear elastic behavior throughout the cycle (solid curves), the deformation sequence was carried out as detailed in Appendix A - Fig. A.6. (f–i) The variations of the cumulative work per unit volume as the chiral metamaterial is deformed through the linear deformation cycle. The work cycles represented by the solid curves are the predictions of the finite element simulations, while the work cycles represented by marks are the predictions of the analytical model based on Eq. (29). The results are represented when the chiral metamaterial was used through the same deformation sequence, while spatially inverting the dilation $\gamma_1 = \pm 0.0125$ and the rotation $\gamma_2 = \pm 0.0125$. The mechanical work that can be obtained from the deformation cycle is the value of the cumulative work per unit volume in units of kJ/m^3 at the end of the cycle.

and the ligaments are made of Aluminum (elastic modulus $E = 70$ GPa) with 1.5 mm thickness and 30 mm width. To enable nonreciprocity, ligaments were made with local geometrical asymmetries with $\theta_0 = 60°$. Following the same sequence shown in Fig. 5(a), the chiral metamaterial was used through four deformation cycles with different combinations of spatially inverted dilations and rotations, i.e., $\gamma_1 = \pm 0.0125$ and $\gamma_2 = \pm 0.0125$. In each of these deformation cycles, starting from a zero-stress state, the chiral metamaterial underwent a sequence of four elastic (*reversible*) deformation processes, in each of which the energy balance law in Eq. (31) was satisfied. For each of these deformation cycles, the variations of the stresses σ_1 and σ_2 through the cycle were determined as shown in Figs. 5(b)-5(e), while the cumulative work per unit volume W during each cycle was determined by means of analytical solutions based on Eq. (29) (see Appendix B for more details) and finite element simulations using the commercial simulation package ABAQUS (Smith, 2009) (see Appendix A for more details), as shown in Figs. 5(f)-5(i).

As demonstrated above, the chiral metamaterial can exhibit chiral, nonreciprocal elastic response and modulation of its elastic properties, which is dependent on how the contact state between the ligament and the rigid circles changes as the chiral solid is deformed. Therefore, we anticipate that a deformation cycle from which mechanical work can be obtained is one in which the contact state of the chiral solid changes through the deformation cycle—specifically, some processes of the deformation cycle are carried out where no contact is established between the ligaments and the circles, while the other processes are carried out where contact is established between the ligaments and the circles. Therefore, we considered the chiral metamaterial undergoing four closed cycles of dilation–rotation coupling (Figs. 5(b)-5(e)). In two of these cycles (shown in Figs. 5(b) and (d)), the contact state changes during the deformation cycle, while in two of these cycles (shown in Figs. 5(c) and (e)), the contact state does not change during the deformation cycle. However, there are some practical challenges with carrying out these deformation cycles, as certain actions must be taken to ensure the mechanical response of the chiral metamaterial is linear and chiral, nonreciprocal elastic, and thus we make several remarks here on how to choose and establish a deformation cycle in which the chiral metamaterial can reveal mechanical activity.

First, to obtain mechanical work from deforming the chiral metamaterial through a closed deformation cycle, the contact state between the ligaments and the circles must change during the deformation cycle, as this enables the modulation of the elastic properties of the chiral solid, and thus chiral, nonreciprocal elasticity.

Second, according to Eq. (35), the mechanical behavior of the chiral metamaterial must be linear elastic through each process of the deformation cycle in order to obtain non-zero mechanical work, and this requires a specific contact state between the ligaments and the circles to be established for each deformation process, and further that this contact state be maintained constant through the deformation process.

Third, the transition between two different contact states should be done at the end of a deformation process, not during a deformation process. This is required to ensure linear mechanical response of the chiral metamaterial, as a nonlinear mechanical response is obtained when a transition between two different contact states occurs during a deformation process (see the dotted curves in Figs. 5(b)-5(e)).

Fourth, the values of the applied deformation fields should be chosen to give non-zero mechanical work, as according to Eq. (35), for each deformation cycle, there is a specific combination of the coupled deformation fields at which the mechanical work for a linear chiral, nonreciprocal elastic solid (i.e., with non-zero β and λ_i) is zero. For instance, for a dilation–rotation cycle ($\lambda_1 \Leftrightarrow \lambda_2$) starting from zero-stress state, the mechanical work is zero when the chiral solid is deformed such that the ligaments are detached from the circles in the first two processes (no contact), and then full contact is established between the entire curved end of each ligament and the circles at the end of the second deformation process, as this deformation sequence requires $\gamma_1/\gamma_2 = (2\beta \pm \sqrt{4\beta^2 + \lambda_1\lambda_2})/\lambda_1$, which gives zero mechanical work according to Eq. (35) (see Appendix B for more details).

To comply with the aforementioned requirements, the dilation–rotation cycle shown in Fig. 5(b), where the chiral metamaterial was deformed by $\gamma_1 = -0.0125$ and $\gamma_2 = -0.0125$ in two consecutive processes and then reversed in another two consecutive processes, was carried out such that, in the first two processes ($1 \rightarrow 2$ and $2 \rightarrow 3$), the ligaments are detached from the rigid circles, while after Process $3 \rightarrow 4$ and at State 4, full contact is established between the ligaments and the circles, such that the entire curved end of the ligament is pressed against the circular profile of the rigid circle. To avoid having nonlinear mechanical response due to a transition from a no contact state to a full contact state during Process $3 \rightarrow 4$, we established at State 3 and before undergoing Process $3 \rightarrow 4$ a specific area of contact between the curved end of the ligament and the circle that gives linear mechanical behavior through Process $3 \rightarrow 4$, and which also leads to the state of stress at the end of the deformation cycle being zero. These different contact states can be achieved by enabling the chiral structure a mechanism of changing the profile of the circle to establish at State 3 a contact angle of 19.7° between the ligaments and the circles, and then to establish at State 4 contact angle of 60° between the ligaments and the circles (see Fig. A.6 - Appendix A for more details). The change in the contact state of the chiral metamaterial during the deformation cycle enables it to exhibit chiral, nonreciprocal elasticity (see Fig. 5(b)), and thus the mechanical work was determined by the value of the cumulative work at the end of the deformation cycle by $W \cong 16.6\ \text{kJ/m}^3$, as shown in Fig. 5(f). We note that the contact angle 19.7° is specific for the applied deformations $\gamma_1 = -0.0125$ and $\gamma_2 = -0.0125$, as this contact state was determined to give the state of stress of the chiral solid zero at the end of the deformation cycle.

We emphasize that the change in the contact state of the chiral metamaterial was achieved without contributing any energy gain/loss to the solid, as the state of stress of the chiral solid does not change when we change the contact state at State 3 or State 4, as shown in Fig. 5(b). Here, we adopted an approach of changing the contact state by changing the circle profile (see Fig. A.6 - Appendix A), which can be practically done by means of a rigid-body slider mechanism, where the circumferential profile of the circle changes by the rigid motion of a slider up and down, that – importantly – must not change the state of stress of the chiral solid when applied, and thus it does not contribute any energy to the chiral solid. This mechanism of changing the circle profile is still part of the mechanism required to modulate the elastic stiffness of the considered chiral metamaterial by changing the contact state (see Figs. 3 and 4).

Similar actions were also taken to change the contact state of the chiral metamaterial through the dilation–rotation cycle shown in Fig. 5(d), in which the chiral solid was first deformed by $\gamma_1 = +0.0125$ and $\gamma_2 = +0.0125$ in two processes, and then the deformation was reversed in the last two processes (see Fig. A.6 - Appendix A). After the first two processes ($1 \rightarrow 2$ and $2 \rightarrow 3$), where full contact is established between the ligaments and the circles (60° of contact angle), we changed the contact state to only 12.5° before undergoing Process $3 \rightarrow 4$ and at State 3. Then, after Process $3 \rightarrow 4$ and at State 4, the contact between the ligaments and the circles was removed, where no contact was established during Process $4 \rightarrow 1$. Through this deformation cycle, the chiral metamaterial revealed chiral, nonreciprocal elasticity (see Fig. 5(d)), and revealed mechanical work of $W = -16\ \text{kJ/m}^3$, as shown in Fig. 5(h). Again, we emphasize that there is no energy gain/loss was contributed anywhere in the deformation cycle.

Comparing these two deformation cycles to the other deformation cycles shown in Figs. 5(c) and 5(e), it follows that the chiral, nonreciprocal elastic response of the chiral metamaterial is suppressed, and thus zero mechanical work was obtained for these deformation cycles, as shown in Figs. 5(g) and 5(i). In these deformation cycles, the chiral structure is deformed such that the ligaments are either detached from the circles (as for the cycle in Fig. 5(c)) or establish full contact of 60° with the circles (as for the cycle in Fig. 5(e)) throughout the entire deformation cycle. Thus, the contact state of the chiral structure does not change through the deformation cycle, and thus no chiral, nonreciprocal elastic behavior can be developed, suppressing the mechanical activity of the chiral solid.

4.2.1. Demonstration of a deformation cycle

To understand how the mechanical work can be developed when deforming the chiral metamaterial through a dilation–rotation closed cycle, while elucidating how this would be related to the chiral, nonreciprocal elasticity of the chiral solid, we focus our discussion here on the deformation cycle shown in Figs. 5(b) and 5(f), in which the chiral metamaterial undergoes a sequence of

compressive dilation $\gamma_1 = -0.0125$ and counterclockwise rotation $\gamma_2 = -0.0125$. Specifically, in Process $1 \to 2$, a uniform compressive dilation $\gamma_1 = -0.0125$ mm/mm is applied, and according to Eq. (29), a dilatational stress $\sigma_1 = \hat{B}\gamma_1$ is developed in the chiral metamaterial, while because of the chirality, the chiral metamaterial also develops a torsional stress $\sigma_2 = -(\hat{A} - \beta)\gamma_1$ that depends on the chiral moduli $\hat{A}$ and β (see Fig. 5(b)). As work depends on the deformation path, the work done on the chiral metamaterial in this process ($W_{1\to2}$) is calculated by the area under the stress σ_1-strain γ_1 curve of the Process $1 \to 2$ in Fig. 5(b) such that $W_{1\to2} = 0.5\int_0^{\gamma_1}(\sigma_1|_{\gamma_2=0})\delta\gamma_1 = 0.25\hat{B}\gamma_1^2$. It is important to note that the limits of the integral of $W_{1\to2}$ expression increase from zero to γ_1, and thus the work $W_{1\to2}$ is done on the chiral solid from its surrounding via the applied compression.

In Process $2 \to 3$, a counterclockwise rotation $\gamma_2 = -0.0125$ is then applied where the torsional stress changes to become $\sigma_2 = -(\hat{A} - \beta)\gamma_1 + (\hat{C} + \lambda_2)\gamma_2$, while through the chiral, nonreciprocal elasticity an additional dilatational stress that depends on the chiral moduli $\hat{A}$ and β and the nonreciprocal modulus λ_1 is also developed, where the overall dilatational stress in the chiral metamaterial becomes $\sigma_1 = (\hat{B}+\lambda_1)\gamma_1 - (\hat{A}+\beta)\gamma_2$. It should be noted that the moduli λ_1 and λ_2 appear in the stress equations because the chiral solid in Process $2 \to 3$ becomes deformed with both dilation and rotation, which are coupled deformation fields. The work done on the chiral metamaterial through the Process $2 \to 3$ can be calculated by the area under the stress σ_2-strain γ_2 curve such that $W_{2\to3} = 0.5\int_0^{\gamma_2}\sigma_2\delta\gamma_2 = -0.5(\hat{A} - \beta)\gamma_1\gamma_2 + 0.25(\hat{C} + \lambda_2)\gamma_2^2$ (see Figs. 5(b) and 5(f)).

In Process $3 \to 4$, the dilation γ_1 is reversed, and thus both the dilatational σ_1 and torsional σ_2 stresses change. If the chiral solid is reciprocal, we anticipate that the same stresses that have been developed in Process $1 \to 2$ are conserved in Process $3 \to 4$. However, because of the chiral, nonreciprocal elasticity of the solid metamaterial, the dilatational stress reversed in Process $3 \to 4$ is different from that which was developed in Process $1 \to 2$ by $\lambda_1\gamma_1$, and thus the dilatational stress at the end of this process becomes $\sigma_1 = -(\hat{A} + \beta)\gamma_2$. Similarly, the torsional stress reversed in Process $3 \to 4$ is also different from that which was developed in Process $1 \to 2$ by $\lambda_2\gamma_2$, such that the conserved torsional stress is $-(\hat{A} - \beta)\gamma_1 + \lambda_2\gamma_2$, and thus the torsional stress at the end of this process becomes $\sigma_2 = \hat{C}\gamma_2$ (see Fig. 5(b)). The work reversed from the chiral metamaterial by the reversal of the dilation γ_1 can be calculated by the area under the stress σ_1-strain γ_1 curve of Process $3 \to 4$ in Fig. 5(b) such that $W_{3\to4} = 0.5\int_{\gamma_1}^{0}\sigma_1\delta\gamma_1 = -0.25(\hat{B} + \lambda_1)\gamma_1^2 + 0.5(\hat{A} + \beta)\gamma_2\gamma_1$. It should be noted that the limits of the integral are swapped, as the dilation is reversed, and thus the work $W_{3\to4}$ is reversed from the chiral solid to the surrounding by removing the prescribed compression.

In Process $4 \to 1$, the rotation γ_2 is reversed, and the stresses drop to zero, and thus the chiral metamaterial recovers its original state by the completion of the deformation cycle, indicating that the deformation cycle is closed. The work reversed from the chiral metamaterial after this process is calculated by the area under the stress σ_2-strain γ_2 curve of the Process $4 \to 1$ in Fig. 5(b) such that $W_{4\to1} = 0.5\int_{\gamma_2}^{0}(\sigma_2|_{\gamma_1=0})\delta\gamma_2 = -0.25\hat{C}\gamma_2^2$.

It follows from these four deformation processes that in the first two processes, work is done on the chiral solid from the surrounding due to external loads applied at the solid's external boundary, which is then reversed from the solid to the surrounding in the last two processes by the removal of the external loads. If the work reversed from the chiral solid to the surrounding is the same as the work done on the chiral solid from the surrounding, the energy used to drive the chiral solid through the deformation cycle is conserved, and it is not conserved otherwise. It follows from the calculations of the deformation processes that the total work done on the chiral solid from the surrounding in Processes $1 \to 2$ and $2 \to 3$ is $W_{in} = W_{1\to2} + W_{2\to3} = 0.25\hat{B}\gamma_1^2 - 0.5(\hat{A} - \beta)\gamma_1\gamma_2 + 0.25(\hat{C} + \lambda_2)\gamma_2^2$, while the work reversed from the chiral solid to the surrounding after Processes $3 \to 4$ and $4 \to 1$ is $W_{out} = W_{3\to4} + W_{4\to1} = -0.25(\hat{B} + \lambda_1)\gamma_1^2 + 0.5(\hat{A} + \beta)\gamma_2\gamma_1 - 0.25\hat{C}\gamma_2^2$. Putting these work values together, it follows that the chiral solid does not conserve energy, as the input work W_{in} is not equal to the output work W_{out} during the deformation cycle, and thus mechanical work can be obtained from this deformation cycle that is $W = W_{in} + W_{out} = -0.25\lambda_1\gamma_1^2 + \beta\gamma_1\gamma_2 + 0.25\lambda_2\gamma_2^2$. For this specific deformation cycle, the cumulative work per unit volume W at the end of the cycle is obtained by $W \cong 16.6$ kJ/m^3, as shown in Fig. 5(f).

It important to note the difference between the cumulative work of our chiral, nonreciprocal elastic metamaterial and the cumulative work of an odd elastic solid (Scheibner et al., 2020) undergoing the same deformation cycle. For the odd elastic solid, where only Form I of chiral nonreciprocity is developed, the cumulative work equals the area of the deformation space $\gamma_1\gamma_2$ times the chiral modulus of non-symmetric elasticity β, i.e., $W = \beta\gamma_1\gamma_2$. However, enabled by not only Form I of chiral nonreciprocity due to the modulus β but also Form II of chiral nonreciprocity due to the moduli λ_1 and λ_2, the cumulative work of our chiral metamaterial depends on the deformation space and the nonreciprocal modulation of the elastic properties.

4.3. Conservation of momenta

Having demonstrated its mechanical activity and chiral, nonreciprocal elasticity, here we investigate the conservation of momenta of the chiral metamaterial. The various momenta of continua with internal spin fields can be defined, as follows:

$$\begin{aligned} &\text{Linear Momentum}: \mathbf{L} = \int_V (\hat{\rho}\dot{\mathbf{u}}(\mathbf{x}))\,\mathrm{d}V \\ &\text{Total Angular Momentum}: \mathbf{J} = \boldsymbol{\Omega} + \mathbf{S}, \text{i.e.,} \\ &\boldsymbol{\Omega} = \int_V (\mathbf{X}(\mathbf{x}) \times \hat{\rho}\dot{\mathbf{u}}(\mathbf{x}))\,\mathrm{d}V \quad \& \quad \mathbf{S} = \int_V \left(\hat{\mathbf{I}} \bullet \dot{\boldsymbol{\Theta}}(\mathbf{x})\right)\mathrm{d}V \end{aligned} \tag{36}$$

where $\dot{\mathbf{u}}$ and $\dot{\boldsymbol{\Theta}}$ are, respectively, the linear velocity of motion and the local, spin velocity of a material particle at point $\mathbf{x}$, $\hat{\rho}$ is the mass density and $\hat{\mathbf{I}}$ is the vector of mass-spin inertia density, and $\mathbf{X}$ is the position vector of the material particle at $\mathbf{x}$ and V is the material volume. In addition to the linear momentum of the particle's motion $\mathbf{L}$, the solid has the total angular momentum $\mathbf{J}$, which is the sum of the orbital angular momentum $\boldsymbol{\Omega}$ of the orbital rotation of each material particle about the material's reference, and the spin angular momentum $\mathbf{S}$ of the independent spinning of each material particle about its mass-center point. The momentum conservation is contingent on the linear momentum $\mathbf{L}$ and the total angular momentum $\mathbf{J}$ remaining constant over time as the solid deforms.

For our chiral metamaterial, every particle can move with u_x and u_y and can also locally spin with θ_z. Considering these independent degrees of freedom, the conservation of linear momentum requires $\dot{L}_k = \int_V (\hat{\rho}\ddot{u}_k)\mathrm{d}V = 0$, and the conservation of total angular momentum requires $\dot{J}_z = \int_V (X_j\epsilon_{jk}\hat{\rho}\ddot{u}_k + \hat{J}\ddot{\theta}_z)\mathrm{d}V = 0$. With the substitution of Eq. (25) into these two expressions, the following conditions of conservation of momenta can be determined:

$$\begin{aligned} \dot{L}_k = 0 \Rightarrow \tau_{ji,j} = 0 \\ \dot{J}_z = 0 \Rightarrow \epsilon_{jk}\tau_{jk} + s_z + m_{i,i} = 0 \end{aligned} \tag{37}$$

According to Eq. (37), the linear momentum and the total angular momentum are both conserved when the chiral metamaterial is deformed quasistatically without any external body forces or external body torques acting on it.

The chiral metamaterial can be deformed while conserving both linear and angular momenta, or while conserving only linear momentum. Under both cases, the chiral metamaterial can still reveal chiral, nonreciprocal elasticity. In the previous demonstrations of the mechanical response of the chiral metamaterial (Figs. 4 and 5), it was deformed while angular momentum was not conserved. For instance, when the chiral metamaterial is used through dilation-(rotation or spin) deformation cycles (e.g., Fig. 5), only linear momentum can be conserved, while the angular momentum is not conserved by the need for the body torque $\sigma_2 \neq 0$ to achieve chiral coupling between dilation and either rotation or spin. Under dilation-(rotation or spin) cycles, a body torque is developed by either rotating the external boundary or by spinning the circles of the chiral metamaterial, and thus the total angular momentum is not conserved $\dot{J}_z \neq 0$. It is important to note that the observed mechanical activity of the chiral metamaterial in Fig. 5 is not due to the non-conservation of the angular momentum, but is instead only due to the chiral, nonreciprocal elasticity of the chiral metamaterial. This can be demonstrated by the zero mechanical work that was obtained when the chiral metamaterial was deformed through the deformation cycles in Figs. 5(c) and 5(e), where despite the angular momentum not being conserved, the chiral metamaterial is reciprocal elastic and gives zero mechanical work. The non-conservation of angular momentum is manifested in the elasticity tensor shown in Eq. (29), as the angular momentum is not conserved if and only if the stress $\sigma_2 \neq 0$.

The chiral metamaterial can also reveal chiral, nonreciprocal elasticity while conserving both linear and angular momenta. The chiral metamaterial conserves angular momentum when deformed such that $\sigma_2 = 0$. This can be achieved by – for example – deforming the chiral metamaterial while letting all circles of the chiral structure to spin freely. When no couple stresses are developed (i.e., $m_i = 0$), according to Eqs. (26) and (37), the total, spin, and orbital angular momenta are all conserved if the stress tensor τ_{ij} is symmetric, i.e., $\epsilon_{jk}\tau_{jk} = 0$. For our chiral metamaterial, the symmetry of the stress tensor can be verified by expressing it in terms of the spin field. Under conservation of spin angular momentum, the uniform spin field can be determined from Eq. (24) as $\theta_z = 0.5(u_{y,x} - u_{x,y}) + ((\hat{\xi}_2 + \kappa_2)/(2(\hat{C} + \lambda_2)))(u_{x,x} + u_{y,y})$, where $\theta_{z,i} = 0$. The substitution of this expression into Eq. (27) gives the stress components in the form:

$$\begin{aligned} \tau_{xx} &= (\hat{B} + \lambda_1)u_{x,x} + \tfrac{1}{2}(\hat{\xi}_1 + \kappa_1)(u_{y,x} + u_{x,y}) - \tfrac{(\hat{\xi}_1+\kappa_1)(\hat{\xi}_2+\kappa_2)}{2(\hat{C}+\lambda_2)}(u_{x,x} + u_{y,y}) \\ \tau_{yy} &= (\hat{B} + \lambda_1)u_{y,y} - \tfrac{1}{2}(\hat{\xi}_1 + \kappa_1)(u_{y,x} + u_{x,y}) - \tfrac{(\hat{\xi}_1+\kappa_1)(\hat{\xi}_2+\kappa_2)}{2(\hat{C}+\lambda_2)}(u_{x,x} + u_{y,y}) \\ \tau_{xy} &= \tau_{yx} = \tfrac{1}{2}(\hat{C} + \lambda_2)(u_{y,x} + u_{x,y}) + \tfrac{1}{2}(\hat{\xi}_2 + \kappa_2)(u_{x,x} - u_{y,y}) \end{aligned} \tag{38}$$

where the stress tensor is symmetric, i.e., $\tau_{xy} = \tau_{yx}$, and thus the total angular momentum is conserved. After the substitution of these stress components into Eq. (30), the constitutive law in Eq. (29) takes the form:

$$\begin{Bmatrix} \sigma_1 \\ \sigma_2 \\ \sigma_3 \\ \sigma_4 \end{Bmatrix} = \begin{bmatrix} \hat{B} - \frac{\hat{\xi}_1\hat{\xi}_2}{\hat{C}} & 0 & 0 & 0 \\ 0 & 0 & 0 & 0 \\ 0 & 0 & \hat{B} + \lambda_1 & \hat{A} + \beta \\ 0 & 0 & \hat{A} - \beta & \hat{C} + \lambda_2 \end{bmatrix} \begin{Bmatrix} u_{x,x} + u_{y,y} \\ u_{x,y} - u_{y,x} \\ u_{x,x} - u_{y,y} \\ u_{x,y} + u_{y,x} \end{Bmatrix} \tag{39}$$

It is clear that the angular momentum is conserved in the elasticity tensor shown in Eq. (39), as the body torque field $\sigma_2 = 0$, and thus it conserves linear momentum along with the various angular momenta. In addition, the elasticity tensor in Eq. (39) is still chiral, nonreciprocal by having the moduli β, λ_1 and λ_2 non-zero and by being asymmetric elastic.

5. Comparison with existing elasticity models

5.1. Chiral, nonreciprocal elasticity versus odd elasticity

Recently, the theoretical construct of odd elasticity was introduced to describe a class of linear elastic, isotropic solids whose constitutive behavior cannot be derived from a free energy (Scheibner et al., 2020). Because of this, the elasticity tensor of an odd elastic solid is not symmetric, and furthermore while odd elastic solids conserve linear momentum, they are not required to conserve angular momentum or energy, and thus they can violate energy conservation as the material is deformed through a closed deformation cycle (Scheibner et al., 2020). Furthermore, the constitutive law of odd elasticity represents the stress as a linear function of the displacement gradient. Thus, there are similarities between the chiral, nonreciprocal elastic constitutive law that we developed here and the odd elasticity proposed by Scheibner et al. (2020). To more easily compare between these two elasticity

concepts, the elasticity tensor of chiral, nonreciprocal elasticity shown in Eq. (11) $C^{\mathrm{cn}}_{\alpha\beta}$ is compared with the elasticity tensor of odd elasticity $C^{\mathrm{odd}}_{\alpha\beta}$, as follows:

$$C^{\mathrm{cn}}_{\alpha\beta}=\begin{bmatrix} \hat{B}_1^{\pm}+\lambda_1^{\pm} & \hat{A}^{\pm}+\beta_1^{\pm} & 0 & 0 \\ \hat{A}^{\pm}-\beta_1^{\pm} & \hat{C}^{\pm}+\lambda_2^{\pm} & 0 & 0 \\ 0 & 0 & \hat{B}_2^{\pm}+\lambda_3^{\pm} & \hat{K}^{\pm}+\beta_2^{\pm} \\ 0 & 0 & \hat{K}^{\pm}-\beta_2^{\pm} & \hat{\mu}^{\pm}+\lambda_4^{\pm} \end{bmatrix} \quad \& \quad C^{\mathrm{odd}}_{\alpha\beta}=\begin{bmatrix} \hat{B}_1 & 0 & 0 & 0 \\ \hat{A} & 0 & 0 & 0 \\ 0 & 0 & \hat{B}_2 & \hat{K} \\ 0 & 0 & -\hat{K} & \hat{\mu} \end{bmatrix} \tag{40}$$

Odd elasticity is capable of breaking reciprocity like chiral, nonreciprocal elasticity by enabling only Form I of chiral nonreciprocity. For instance, the odd elasticity tensor $C^{\mathrm{odd}}_{\alpha\beta}$ models nonreciprocal coupling between dilation and rotation through the odd elastic modulus $\hat{A}$, such that dilation γ_1 produces dilatational σ_1 and torsional σ_2 stresses, while rotation does not produce any stress, while it also models nonreciprocal coupling between dilation and shear through the odd elastic modulus $\hat{K}$, such that the positive dilation gives positive shear while the positive shear gives negative dilation (see Eq. (40)). This is analogous to Form I of chiral, nonreciprocal elasticity we demonstrate in Figs. 1(b) and 1(c). Thus, both elasticity concepts can describe the asymmetric elasticity of matter, where the elasticity tensor is asymmetric in their constitutive laws, and both elasticity tensors are chiral for 2D isotropic solids. Therefore, both concepts cannot be derived assuming a free energy, and because of this, both odd elastic and chiral, nonreciprocal elastic solids can act as sources of mechanical work when used through closed cycles of coupled deformations.

Despite the aforementioned similarities between chiral, nonreciprocal elasticity and odd elasticity around the asymmetric elasticity, the two concepts are still distinct practically and theoretically. The major practical difference between odd elasticity and chiral, nonreciprocal elasticity is that current manifestations of odd elasticity require the use of active elements operated by external, independent energy sources, while chiral, nonreciprocal elasticity can be manifested using passive elements. Specifically, previous realizations of odd elastic solids (Chen et al., 2021b; Scheibner et al., 2020) used internal, active elements with independent energy sources to enable the nonreciprocal coupling needed to get the asymmetric elasticity tensor. For example, piezoelectric actuators and sensors that achieved coupling between bending and shear were used along with an independent energy supplier with feed-forward control to enable odd elasticity in beams. In this design, energy is supplied to the beam for the bending deformation mode but not for the shear deformation mode, achieving nonreciprocal interactions in which bending induces shear, while shear does not induce bending (Chen et al., 2021b). In addition, in the realization of robotic odd elastic active matter, externally powered-actuators and micro-controllers were used to realize nonreciprocal behavior of linkage mechanisms that can exhibit coupled deformation modes, such that the linkage rotation changes by the spatial inversion of the applied deformation (Brandenbourger et al., 2022). Because the deformation of these odd elastic solids is controlled by external energy sources, such solids do not satisfy the energy balance in Eq. (31). In contrast, chiral, nonreciprocal elasticity demonstrates the constitutive behavior of a class of non-symmetric elastic solids that always satisfy the energy balance in Eq. (31). The chiral, nonreciprocal elasticity enables an asymmetric elasticity tensor by combining nonreciprocity that enables modulation of the elastic properties with chirality that enables coupling between different deformation fields, without active elements that require external energy sources. Among the various routes to breaking reciprocity, there are passive, time-invariant media that can also break reciprocity (Asadchy et al., 2020; Coulais et al., 2017; Mahmoud et al., 2015), and thus the realization of nonreciprocity does not always require active media. By implementing a geometrical asymmetry, we realized a chiral metamaterial that exhibits asymmetric elasticity enabled by the modulation of the stiffness of its chiral elements depending on the direction and type of the applied deformation. Therefore, by combining nonreciprocity that enables modulation of the material stiffness with chirality, chiral, nonreciprocal elastic and mechanically active solids can be realized using passive structures, as shown in this work.

The major theoretical difference between chiral, nonreciprocal elasticity and odd elasticity is in the distinct constitutive laws and elasticity tensors (see Eq. (40)). The elastic moduli of the chiral, nonreciprocal elasticity tensor $C^{\mathrm{cn}}_{\alpha\beta}$ are spontaneously modulated by (1) the spatial inversion of the applied deformation (see the ($\pm$) superscripts in Eq. (40)), and (2) by coupling between different deformation fields, as manifested in the moduli λ_i that are developed only when the chiral solid is deformed by coupled deformation fields. This is in contrast to odd elastic solids, where the elastic moduli of the odd elasticity tensor $C^{\mathrm{odd}}_{\alpha\beta}$ are constants and do not vary depending on the direction or mode of deformation of the odd elastic solid. Furthermore, the coupling of chirality and nonreciprocity that is manifested in the chiral, nonreciprocal elasticity tensor $C^{\mathrm{cn}}_{\alpha\beta}$ enables, in addition to the activity due to asymmetric elasticity that is manifested in the odd elasticity tensor $C^{\mathrm{odd}}_{\alpha\beta}$ (Form I of chiral, nonreciprocity through β_i), activity due to the modulation of the material elastic properties depending on the direction and type of the applied deformation (Form II of chiral, nonreciprocity through λ_i). Therefore, the present formulation of chiral, nonreciprocal elastic solids is more general as compared to the formulation of the odd elasticity in previous works (Scheibner et al., 2020).

5.2. Comparison with micropolar continuum models

As the chiral metamaterial exhibits a spin field θ_z by rotating the circles of the chiral structure, the developed chiral, nonreciprocal elasticity of the chiral metamaterial can be compared with micropolar elasticity. Previous works have used micropolar elasticity to model the mechanics of chiral solids (Liu et al., 2012; Joumaa and Ostoja-Starzewski, 2011; Lakes and Benedict, 1982; Lakes, 2001; Natroshvili and Stratis, 2006; Frenzel et al., 2017, 2019; Chen et al., 2020, 2021a). In some of these works, micropolar elasticity was also used to justify the mechanical activity of chiral metamaterials (Frenzel et al., 2017, 2019; Chen et al., 2021a). However, because micropolar elasticity is based on a free energy function and thus enforces energy conservation, the activity described above cannot be captured by the conventional micropolar models. This can be demonstrated by considering the non-centrosymmetric

micropolar model of chiral solids (Lakes, 2001; Liu et al., 2012; Natroshvili and Stratis, 2006; Lakes and Benedict, 1982; Joumaa and Ostoja-Starzewski, 2011), which assumes the following free energy function, for 2D isotropic linear elastic materials (assuming a uniform spin field θ_z) (Liu et al., 2012):

$$w = \frac{1}{2}(\lambda\gamma_{\alpha\alpha}\gamma_{\beta\beta} + \mu_1\gamma_{\alpha\beta}\gamma_{\alpha\beta} + \mu_2\gamma_{\alpha\beta}\gamma_{\beta\alpha}) + A(\gamma_{kk}\epsilon_{\alpha\beta}\gamma_{\alpha\beta}) \tag{41}$$

where $\gamma_{\alpha\beta} = u_{\beta,\alpha} + \epsilon_{\beta\alpha}\theta_z$, and λ, μ_1, and μ_2 are Lame constants, while A is an elastic modulus of chiral coupling. Using the stresses and kinematic variables in Eq. (30), the constitutive law can be then obtained in the following form, according to Eq. (41):

$$\begin{Bmatrix} \sigma_1 \\ \sigma_2 \\ \sigma_3 \\ \sigma_4 \end{Bmatrix} = \begin{bmatrix} 2\lambda+\mu_1+\mu_2 & -2A & 0 & 0 \\ -2A & \mu_1-\mu_2 & 0 & 0 \\ 0 & 0 & \mu_1+\mu_2 & 0 \\ 0 & 0 & 0 & \mu_1+\mu_2 \end{bmatrix} \begin{Bmatrix} \gamma_{xx}+\gamma_{yy} \\ \gamma_{yx}-\gamma_{xy} \\ \gamma_{xx}-\gamma_{yy} \\ \gamma_{xy}+\gamma_{yx} \end{Bmatrix} \tag{42}$$

This micropolar model reveals chiral coupling where the elasticity tensor in Eq. (42) is chiral when the modulus $A \neq 0$. This chirality enables unusual deformations, where dilation produces twist and where twist produces dilation (Liu et al., 2012). However, these unusual deformations do not necessarily entail that the chiral solid is mechanically active, as these deformations are fully recovered by means of energy conservation, and the chiral solid is still mechanically passive if the chirality is not combined with nonreciprocity. As we demonstrated in this study, the mechanical activity of chiral solids is contingent on having chiral nonreciprocity, and thus the verification of the mechanical activity of chiral metamaterials should be carried out based on energy conservation and chiral, nonreciprocal elasticity rather than the material deformation. The elasticity tensor in Eq. (42) is reciprocal, as it is symmetric and with constant elastic moduli, and therefore it cannot reveal chiral, nonreciprocal elasticity or mechanical activity under static equilibrium. Therefore, further justifications may be needed on the mechanical activity of chiral metamaterials considered in studies, e.g., Frenzel et al. (2017), Frenzel et al. (2019) and Chen et al. (2021a), where the verification of the mechanical activity was carried out based on measures other than chiral nonreciprocity, e.g., unusual twist and unusual acoustic phonons.

Another micropolar elasticity model that enforces non-conservation of angular momentum has been developed and used to make elastic cloaks (Vasquez et al., 2012; Nassar et al., 2020a, 2019; Zhang et al., 2020; Xu et al., 2020), by exploiting the resulting non-symmetric stress tensor to enable cloaking without requiring anisotropy. In the context of this model, the chiral solid is assumed working under an external angular momentum source that produces an external body torque – that is a linear function of the spin θ_z – acting on the solid. This external body torque adds torsional stiffness C^E to the component C_{22} of the elasticity tensor in Eq. (42), such that it becomes $C_{22} = \mu_1 - \mu_2 + C^E$. With this, the orbital angular momentum is not conserved, and thus the stress tensor that is based only on the displacement gradient is asymmetric, while because the external torque only contributes to a diagonal element of the elasticity tensor, the elasticity is still reciprocal and symmetric, and therefore this micropolar model cannot reveal non-symmetric elasticity or mechanical activity.

In the same context, it is important stating the case when the chiral solid is connected to an external, independent energy source that produces momentum contributing to the dilation–rotation coupling of the solid. If this source of external momentum is reciprocal, it produces an external body torque $T^E = 2A^E(\gamma_{xx}+\gamma_{yy})$, while it also produces external body forces $F^E_x = 2A^E(\gamma_{xy,x}-\gamma_{yy,y})$ and $F^E_y = 2A^E(\gamma_{xx,x} - \gamma_{yx,y})$, all of which are equivalently coupled via the same coupling modulus A^E. Under this reciprocal momentum, the constitutive law of the micropolar continuum takes the following form:

$$\begin{Bmatrix} \sigma_1 \\ \sigma_2 \\ \sigma_3 \\ \sigma_4 \end{Bmatrix} = \begin{bmatrix} 2\lambda+\mu_1+\mu_2 & -2(A+A^E) & 0 & 0 \\ -2(A+A^E) & \mu_1-\mu_2 & 0 & 0 \\ 0 & 0 & \mu_1+\mu_2 & 2A^E \\ 0 & 0 & 2A^E & \mu_1+\mu_2 \end{bmatrix} \begin{Bmatrix} \gamma_{xx}+\gamma_{yy} \\ \gamma_{yx}-\gamma_{xy} \\ \gamma_{xx}-\gamma_{yy} \\ \gamma_{xy}+\gamma_{yx} \end{Bmatrix} \tag{43}$$

It is clear that, under reciprocal external momentum sources, the elasticity tensor is symmetric, and thus it cannot reveal chiral, nonreciprocal elasticity or mechanical activity. For the elasticity tensor to be asymmetric, the momentum source should be nonreciprocal such that it develops either body torque or body forces by injecting momentum in only one direction (or at least the force and the torque fields are not equivalently coupled by enabling different coupling moduli). Approaches of enabling asymmetric elasticity based on external momentum sources often require the use of external energy sources along with one-way controllers to realize nonreciprocal momenta (Brandenbourger et al., 2019; Chen et al., 2021b; Scheibner et al., 2020; Brandenbourger et al., 2022). However, by exploiting a geometrical asymmetry that resulted in nonreciprocal elastic behaviors in which the material elastic properties can be modulated depending on the direction of the applied deformation, we demonstrated the enabling of nonreciprocal momenta and asymmetric elasticity in chiral elastic solids without using nonreciprocal, external momentum or energy sources. Specifically, we demonstrated a chiral metamaterial that can spontaneously develop nonreciprocal momenta without using external momentum sources, such that, according to Eqs. (22)–(24), it can develop spontaneous body torque $T^S = (\hat{A} - \beta)(\gamma_{xx} + \gamma_{yy})$ and spontaneous body forces $F^S_x = (\hat{A} + \beta)\gamma_{xy,x} - (\hat{A} - \beta)\gamma_{yy,y}$ and $F^S_y = (\hat{A} - \beta)\gamma_{xx,x} - (\hat{A} + \beta)\gamma_{yx,y}$ during deformation, which are not equivalently coupled to each other by having the nonreciprocal modulus $\beta \neq 0$.

Overall, the constitutive theory based on chiral, nonreciprocal elasticity that we developed to model the chiral metamaterial made of passive elements that can act as a source of mechanical work is distinct from previously developed micropolar elasticity models by (1) modeling the mechanics of chiral solids without the assumption of the existence of a free energy, and thus it can describe situations for which the solid may violate energy conservation, (2) modeling the nonreciprocal behavior of active chiral solids, and in particular the consequences of coupling chirality with nonreciprocity, and (3) enabling mechanical activity using passive structures, with no need for external energy sources.

6. Conclusions

The main contribution of this work is two-fold. First, we have proposed the notion of chiral, nonreciprocal elasticity, which represents a generic route to enabling 2D, isotropic elastic solids exhibiting asymmetric elasticity, and thus such elastic solids can break static thermodynamic equilibrium and can act as sources of mechanical work when used in specific quasistatic deformation cycles. Specifically, this approach describes elastic behaviors that result from coupling nonreciprocity with chirality, to enable the nonreciprocal coupling of different deformation fields, which enables such solids to exhibit: (1) asymmetric isotropic elasticity in which the solid conserves linear momentum, and (2) spontaneous modulations of the elastic properties depending on the mode of deformation. Second, we have developed an isotropic 2D chiral metamaterial that, by exploiting local geometrical asymmetry, behaves in a chiral, nonreciprocal elastic fashion while only requiring passive, and not active energy sources. We have also demonstrated, arising from its asymmetric elasticity, the ability of the chiral metamaterial to act as a source of mechanical work through specific quasistatic deformation cycles though no energy is dissipated/consumed by its passive elements. Furthermore, using finite element simulations we have demonstrated the practical actions that must be taken for the chiral metamaterial to exhibit the idealized linear, chiral nonreciprocal elastic behavior and thus mechanical activity through a quasistatic deformation cycle. Because of the relative simplicity of the chiral metamaterial, we anticipate that the developments made in this work will enable further fundamental investigations into a range of emerging research areas, including solid active matter (Bowick et al., 2022), and topological mechanics (Shankar et al., 2020).

Declaration of competing interest

The authors declare that they have no known competing financial interests or personal relationships that could have appeared to influence the work reported in this paper.

Data availability

Data will be made available on request.

Acknowledgments

The authors acknowledge the support of ARO, United States grant W911NF-21-2-0091.

Appendix A. Finite element simulations

To demonstrate the mechanical response of the chiral metamaterial, and to verify the developed analytical models including the chiral, nonreciprocal constitutive law in Eq. (29), we carried out static finite element simulations – using the commercial simulation package ABAQUS (Smith, 2009) – of the chiral metamaterial in Fig. 2(a) when used through the various deformations shown in Figs. 3–5. To obtain the results presented in this study, we modeled a chiral lattice that is comprised of 4×4 chiral elements with $\alpha_0 = 30°$ chiral angle and $a = 20$ mm lattice constant (Fig. 2). The circles of the chiral lattice were modeled as rigid bodies, while the ligaments were modeled as linear elastic Bernoulli–Euler beam elements with cross sectional dimensions $b = 30$ mm$\times h = 1.5$ mm for a rectangular cross section, where b is the width and h is the thickness, and with Young's modulus $E = 70$ GPa and zero Poisson's ratio. To enable microscopic geometrical asymmetry of the chiral metamaterial, the ligaments were made tangent to the circles with curved ends around the circles with $\theta_0 = 60°$, as shown in Fig. 2(c). Rigid connections were defined between the elastic ligaments and the rigid circles such that the end points of the ligaments were rigidly tied to the circles, as indicated by the tied joints in Fig. 2(c). In addition, a node-to-surface, Augmented Lagrangian hard contact was defined between the ligaments and the circles, where the hard contact was only defined in the normal direction, while there are no tangential frictional or dissipative interactions that were considered.

For all finite element simulations carried out in this work, we adopted assumptions leading to linear elastic mechanical response of the chiral metamaterial, and thus all sources of nonlinearity were eliminated. Specifically, for all simulations, the circles of the chiral lattice were modeled as rigid bodies, while the ligaments were modeled as linear, elastic Bernoulli–Euler beam elements with uniform, rectangular cross section and linear, elastic material properties. In addition, small-displacement/strain analyses were adopted in all simulations, where the geometric nonlinearity was not considered. Furthermore, to maintain the linear elastic response of the chiral metamaterial, while the contact between the ligaments and the circles is considered, we deformed the chiral metamaterial with small displacements and small rotations at the centers of the rigid circles. Specifically, in all simulations presented in this study, the chiral metamaterial was deformed by small strains $u_{i,j} = \pm 0.00625$ and small rotations $\theta_z = \pm 0.0125$, which resulted in linear mechanical response of the chiral metamaterial while the contact was considered, as shown in the stress–strain results in Figs. 4 and 5.

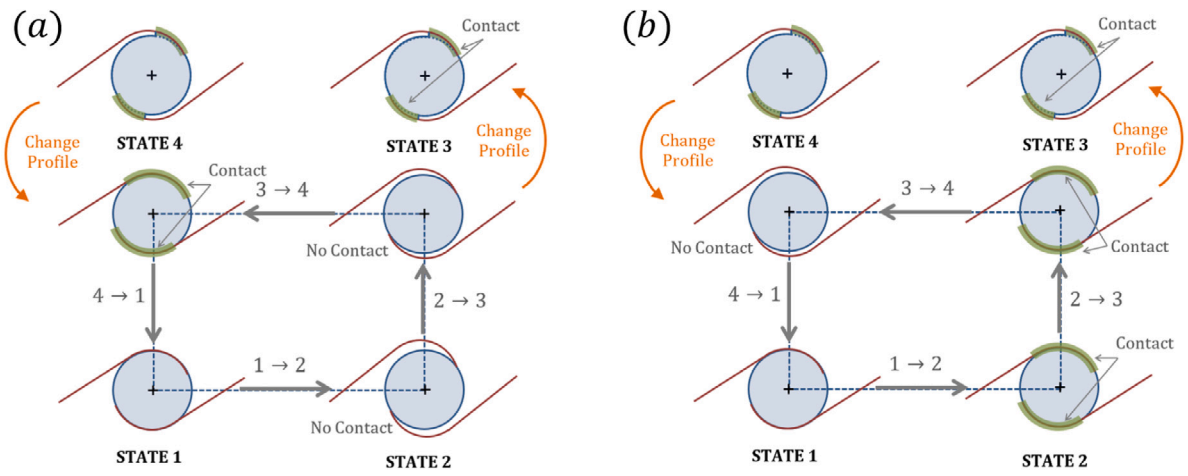

Fig. A.6. Detailed sequence of the quasistatic deformation cycles presented in (a) Fig. 5(b) and (b) Fig. 5(d), elucidating the change in the contact state throughout the deformation cycle. These deformation cycles were carried out such that the profile of the circle was changed at State 3 to establish contact with (a) 19.7° and (b) 12.5° of the ligament's curved end, and then at State 4 the profile was changed to establish (a) full contact of 60° or (b) no contact with the curved end of the ligament.

A.1. Finite element simulations of the chiral metamaterial through quasistatic deformation cycles

The finite element simulation of the chiral metamaterial when used through each one of the quasistatic deformation cycles shown in Fig. 5 was carried out over four deformation steps of static analysis such that two coupled deformation fields were applied in a two consecutive steps, which were then reversed in another two consecutive steps. In each step, the chiral metamaterial was deformed by a uniform deformation field where prescribed displacements or spins were applied at the centers of the rigid circles, as shown in Fig. A.7. The horizontal and vertical nodal forces F_{xm} and F_{ym} and the nodal moment M_{zm} along with the nodal displacements u_{xm} and u_{ym} and the nodal rotations θ_{zm} at the centers of the circles of the chiral lattice were determined with the incremental change of the applied deformation.

As shown in Figs. 5(b) and 5(d), because of nonreciprocity, the chiral metamaterial may undergo a transition between a state where the ligaments are detached from the circles and a state where the ligaments come into full contact with the circles, resulting in a nonlinear mechanical response when the applied deformation is reversed during Process 3 → 4. To obtain linear response during Process 3 → 4, at State 3 and before undergoing Process 3 → 4, a specific contact was established between the ligaments and the circles by changing the circle profile, as shown in Fig. A.6. For instance, after Processes 1 → 2 and 2 → 3 of the deformation cycle shown in Fig. 5(b), the ligaments are detached from the circles. Then at State 3, we change the profile of the circle to establish contact between the ligaments and the circles, as shown in Fig. A.6(a). After Process 3 → 4 (at State 4), we change the profile of the circle again to establish full contact between the curved ends of the ligaments and the circles, as shown. With this, the behavior of the chiral structure is linear elastic throughout the deformation cycle, as shown in Fig. 5(b). It should be noted that the change of the circle profile does not contribute any energy gain/loss to the chiral structure, as the state of stress of the solid does not change by changing the circle profile at State 3 or State 4, as shown in Fig. 5.

Practically, the change of the circle profile can be done utilizing a slider mechanism that moves rigidly up and down to change the circumferential profile of the circle, and thus changes the contact state of the chiral solid. Specifically, at State 3 and before undergoing Process 3 → 4, the slider is moved up rigidly to establish contact with a portion of the curved end of the ligament, and this contact state is maintained during Process 3 → 4. Then, after Process 3 → 4 and at State 4, the slider is displaced back rigidly to establish contact with the entire curved end of the ligament. While this slider would require a mechanism actuating it, it does not contribute any energy gain/loss to the chiral solid as (1) it moves rigidly and (2) it does not change the state of stress of the chiral solid when applied.

To calculate the variation of the internal energy density w of the chiral metamaterial through the deformation cycle, the sum of the nodal forces at the centers of the circles of the top boundary layer $F_{yx}^{(i)} = \sum_{m=1}^{5} F_{xm}$ and $F_{yy}^{(i)} = \sum_{m=1}^{5} F_{ym}$ and at the centers of the circles of the right boundary layer $F_{xx}^{(i)} = \sum_{m=1}^{5} F_{xm}$ and $F_{xy}^{(i)} = \sum_{m=1}^{5} F_{ym}$, and also the sum of the nodal moments at the centers of all circles $M_z^{(i)} = \sum_{m=1}^{25} M_{zm}$ were first determined at all increments of the applied deformation, where the superscript (i) stands for the increment number. Then, the stress components were calculated at every increment, such that the stresses at the ith increment take the form:

$$\begin{aligned} \tau_{xx}^{(i)} &= F_{xx}^{(i)}/4ab \\ \tau_{yy}^{(i)} &= F_{yy}^{(i)}/4ab \\ \tau_{xy}^{(i)} &= F_{xy}^{(i)}/4ab \\ \tau_{yx}^{(i)} &= F_{yx}^{(i)}/4ab \\ \hat{M}^{(i)} &= M_z^{(i)}/16a^2b \end{aligned} \tag{A.1}$$

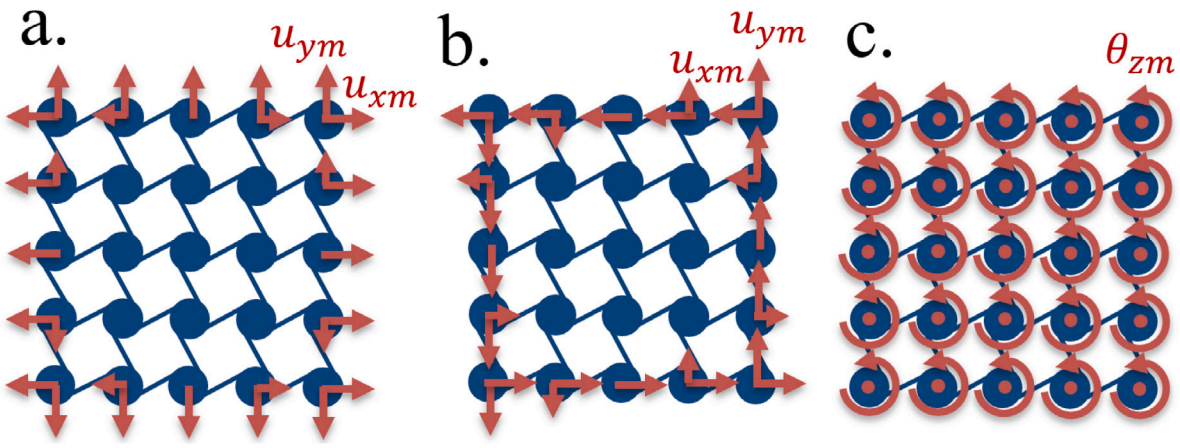

Fig. A.7. Boundary conditions employed in the finite element simulations of the chiral metamaterial. The chiral metamaterial was deformed by (a-b) prescribed displacements u_{xm} and u_{ym} and (c) prescribed spin θ_{zm} at the centers of the rigid circles. In (a-b), u_{xm} and u_{ym} are the nodal displacements defined at the center of the circle, where m stands for the circle index. The displacements were applied at the circles to achieve uniform (a) dilation $\gamma_1 = u_{x,x} + u_{y,y}$ and (b) rotation $\gamma_2 = u_{x,y} - u_{y,x}$. The size of the arrow scales the nodal displacements prescribed at the center of each circle. Circles with dots at their centers were fixed along $x-$ and $y-$directions, such that $u_{xm} = 0$ and $u_{ym} = 0$, while circles without prescribed displacements were allowed to move freely along $x-$ and $y-$directions. The spin θ_{zm} at all circles was maintained fixed such that $\theta_{zm} = 0$ at all circles. In (c), the chiral metamaterial was deformed by uniform spin field such that a spin θ_{zm} was applied at the centers of all circles, while the centers of the circles were fixed along $x-$ and $y-$directions, such that $u_{xm} = 0$ and $u_{ym} = 0$.

Then, the internal energy density w at the ith increment was calculated, as follows (see Eq. (32)):

$$w^{(i)} = \frac{1}{2}\left(\tau_{xx}^{(i)}u_{x,x}^{(i)} + \tau_{yy}^{(i)}u_{y,y}^{(i)} + \tau_{xy}^{(i)}u_{y,x}^{(i)} + \tau_{yx}^{(i)}u_{x,y}^{(i)} + \hat{M}^{(i)}\theta_z^{(i)}\right) \tag{A.2}$$

where the deformations $u_{i,j}^{(i)}$ and $\theta_z^{(i)}$ were calculated, after determining the average of the nodal displacements at the centers of the circles of the top boundary layer $u_{xy}^{(i)} = \sum_{m=1}^{5} u_{xm}/5$ and $u_{yy}^{(i)} = \sum_{m=1}^{5} u_{ym}/5$, and at the centers of the circles of the right boundary layer $u_{xx}^{(i)} = \sum_{m=1}^{5} u_{xm}/5$ and $u_{yx}^{(i)} = \sum_{m=1}^{5} u_{ym}/5$, along with the nodal spin $\theta_z^{(i)} = \sum_{m=1}^{25} \theta_{zm}/25$ at the centers of all circles, as follows:

$$\begin{aligned} u_{x,x}^{(i)} &= u_{xx}^{(i)}/2a \\ u_{y,y}^{(i)} &= u_{yy}^{(i)}/2a \\ u_{x,y}^{(i)} &= u_{xy}^{(i)}/2a \\ u_{y,x}^{(i)} &= u_{yx}^{(i)}/2a \end{aligned} \tag{A.3}$$

To verify the energy balance in Eq. (31) for the chiral metamaterial during the deformation cycle along with the accuracy of the performed simulations, we carried out finite element simulations for each process of the deformation cycle separately and evaluated the values of the various energy terms that ABAQUS uses to determine the energy balance of the entire chiral model, where only two energy terms have been found non-zero through the deformation process, namely the internal energy $\mathrm{d}\psi$ and the external work δW, and thus the variation of the total energy function (i.e., $\delta E_{total} = \mathrm{d}\psi - \delta W$) through each deformation process was determined by $E_{total}^{(i)} \cong 0$ at all increments of the process. This verifies that each deformation process of the deformation cycle was carried out satisfying the energy balance in Eq. (31), which indicates that the chiral solid is deformed without contributing external energy gain/loss to the solid.

It follows from Eq. (A.2) that the internal energy density of the chiral metamaterial is zero at the end of the deformation cycle, as the stresses and all displacements drop to zero when the chiral metamaterial recovers its original undeformed configuration at the end of the cycle, and thus the net change in the internal, free energy of the chiral metamaterial over the deformation cycle is zero (i.e., $\oint_{\partial\Omega} \mathrm{d}\psi = 0$). Nonetheless, while the energy balance in Eq. (31) has to be satisfied for each process of the deformation cycle, mechanical work can still be developed when the chiral metamaterial undergoes and completes the closed deformation cycle. The mechanical work equals the amount of work accumulated by the deformation of the chiral metamaterial through the cycle (i.e., $W = \oint_{\partial\Omega} \delta W \neq 0$). The variation of the cumulative work per unit volume w_c of the chiral metamaterial through the deformation cycle was calculated, as follows:

$$w_c^{(i)} = \sum_{n=1}^{i}\left[\tau_{xx}^{(n)}\left(u_{x,x}^{(n)} - u_{x,x}^{(n-1)}\right) + \tau_{yy}^{(n)}\left(u_{y,y}^{(n)} - u_{y,y}^{(n-1)}\right) + \tau_{xy}^{(n)}\left(u_{y,x}^{(n)} - u_{y,x}^{(n-1)}\right) + \tau_{yx}^{(n)}\left(u_{x,y}^{(n)} - u_{x,y}^{(n-1)}\right) + \hat{M}^{(n)}\left(\theta_z^{(n)} - \theta_z^{(n-1)}\right)\right] \tag{A.4}$$

where $w_c^{(i)}$ is the cumulative work per unit volume at the ith increment. As the deformation cycle was initiated from a zero stress state, the mechanical work W developed by deforming the chiral metamaterial through the closed deformation cycle was then determined by the value of the cumulative work per unit volume at the end of the deformation cycle, such that $W = w_c^{(N)}$, where $N = 40000$ is the number of increments considered through the deformation cycle.

A.2. Determination of the ligament stiffness

Because beams with curved portions exhibit different rigidities depending on the direction of the applied load, analytical computations of the rigidities and the equivalent stiffnesses of the ligaments of the chiral metamaterial could be challenging, and therefore we adopted a numerical approach to determine the equivalent stiffnesses of the ligament $k_{\alpha\beta}$ shown in Eqs. (13) and (15)–(17). Specifically, we carried out static finite element simulations of one ligament connecting two rigid circles (Fig. 2(c)) to determine the equivalent stiffnesses $k_{\alpha\beta}$. The one ligament-two circles structure shown in Fig. 2(c) is the minimal model that can be used to determine the equivalent stiffnesses of the chiral element, as the four ligaments of the chiral element are identical, similarly distributed around the central circle, and exhibit similar deformations (see Fig. 2(b)). This minimal structure was considered under the different deformations shown in Fig. 3, where the circle (i, j) was fixed, while the other circle $(i+1, j)$ was subjected to a displacement u_x or u_y or spin θ_z at its center. The forces F_x and F_y along with the moment M_z at the center $(i+1, j)$ were then determined. Afterwards the equivalent stiffnesses of the ligament were determined by substituting the numerically obtained forces and moment into the following relations:

$$\begin{aligned} F_x &= k_{xx}u_x + k_{xy}u_y - 2k_{x\theta}\theta_z \\ F_y &= k_{yx}u_x + k_{yy}u_y - 2k_{y\theta}\theta_z \\ M_z &= -k_{\theta x}u_x - k_{\theta y}u_y + 2k_{\theta\theta}\theta_z \end{aligned} \tag{A.5}$$

The chiral element reveals directional nonreciprocity (Fig. 1(a)), as the equivalent stiffnesses change by changing the direction of the applied deformation. For example, when the ligament was stretched with $u_x = +0.25$ mm (while $u_y = 0$ and $\theta_z = 0$), the forces $F_x = 21.55$ kN and $F_y = 12.15$ kN were developed, and thus, according to Eq. (A.5), the axial stiffness $k_{xx} = 86.18$ kN/mm and the coupling stiffness $k_{yx} = 48.58$ kN/mm were calculated, as shown in Table A.1. If the structure is reciprocal, we anticipate the same forces are developed when the displacement is spatially inverted. However, the forces were obtained by $F_x = -10.30$ kN and $F_y = -5.06$ kN when the displacement was inverted to $u_x = -0.25$ mm, and thus the stiffnesses k_{xx} and k_{yx} also changed to become $k_{xx} = 41.19$ kN/mm and $k_{yx} = 20.25$ kN/mm, indicating directional nonreciprocity. A similar behavior was observed when calculating the other stiffnesses before and after the inversion of the corresponding, applied deformation.

The chiral element also reveals Form I of chiral nonreciprocity (Figs. 1(b) and 1(c)), where the stiffness matrix of the chiral element was obtained non-symmetric (i.e., $k_{\alpha\beta} \neq k_{\beta\alpha}$). In reciprocal material systems, the symmetric stiffness matrix indicates that the coupling stiffness is the same when the structure is deformed by either one of two coupled deformation fields. However, when the chiral structure was deformed by $u_x = +0.25(-0.25)$ mm, the stiffness of the axial-bending coupling of the ligament was obtained by $k_{yx} = 48.58(20.25)$ kN/mm (Table A.1), which was then changed to $k_{xy} = 48.43(20.25)$ kN/mm when the chiral structure was deformed by $u_y = +0.25(-0.25)$ mm, and this clearly indicates that the axial-bending coupling of the chiral structure is asymmetric when the structure is deformed by $u_x = +0.25$ mm and $u_y = -0.25$ mm, or by $u_x = -0.25$ mm and $u_y = +0.25$ mm. In general, the chiral structure reveals asymmetry for the axial-bending coupling ($k_{xy} \neq k_{yx}$) and the axial-rotation coupling ($k_{\theta x} \neq k_{x\theta}$), while it gives symmetric bending-rotation coupling ($k_{\theta y} \cong k_{y\theta}$).

The stiffness can also change when the chiral element is deformed by two coupled deformation fields instantaneously. This can be verified by comparing the forces developed in the chiral element when it is deformed by each one of the deformation fields to the forces developed in the element when the two deformation fields are both applied instantaneously. For example, the chiral element was considered under three loading cases in which the element is deformed by (1) $u_x = +0.25$ mm only, (2) $u_y = -0.25$ mm only, and by (3) both $u_x = +0.25$ mm and $u_y = -0.25$ mm, where the force F_x developed in the element was determined for each of these cases by 21.55, −5.06, and 9.43 kN, respectively. The axial stiffness $k_{xx}^{(1)} = F_x^{(1)}/u_x$ was then calculated for the first loading case by $k_{xx}^{(1)} = 86.18$ kN/mm. The stiffness k_{xx} can be then calculated for the third loading case by subtracting the contribution of the coupling force $F_x^{(2)}$ from the total force $F_x^{(3)}$ while calculating the stiffness such that $k_{xx}^{(3)} = (F_x^{(3)} - F_x^{(2)})/u_x = (9.43 + 5.06)/0.25 = 57.94$ kN. It is clear that the stiffness value is decreased by 28.24 kN/mm when changing the loading case from deforming the chiral element with only one deformation field to deforming it by two coupled deformation fields, which verifies Form II of chiral nonreciprocity (Fig. 1(d)).

In Table A.1, we give some of the numerically determined stiffnesses of the ligaments, illustrating the modulation of the stiffness of the chiral element depending on the direction and type of the applied deformation.

A.3. Determination of the chiral, nonreciprocal elastic moduli

Here, we show the analytical calculations of the chiral, nonreciprocal elastic moduli shown in Eq. (29) using the stiffnesses calculated via the methodology shown in Appendix A.2. First, we determined the discrete equations of a chiral metamaterial with 4×4 chiral elements in terms of the applied displacements and spins at the centers of the circles, from which we determined the continuum field equations, and then the elastic moduli were obtained in terms of the equivalent stiffnesses $k_{\alpha\beta}$, as follows:

$$\begin{aligned} &\hat{B} + \lambda_1 = 5k_{xx}/4b, \hat{C} + \lambda_2 = 5k_{yy}/4b = 5k_{\theta y}/2ab = 5k_{y\theta}/2ab = 5k_{\theta\theta}/a^2b \\ &\hat{A} = 5(k_{xy} + k_{yx})/8b = 5(k_{x\theta} + k_{\theta x})/4ab, \beta = 5(k_{xy} - k_{yx})/8b = 5(k_{x\theta} - k_{\theta x})/4ab \end{aligned} \tag{A.6}$$

Then, the numerically determined equivalent stiffnesses of the chiral element $k_{\alpha\beta}$ (from Appendix A.2) were substituted into Eq. (A.6), which gave the elastic moduli values, as shown in Table A.2. It should be noted that the calculations of the elastic moduli were carried out while considering the changes of the equivalent stiffnesses depending on the direction of the applied deformation, and whether the chiral metamaterial is deformed by one deformation field or multiple deformation fields.

Table A.1
Examples of numerically determined equivalent stiffnesses of the ligaments of a chiral metamaterial with $\alpha_0 = 30°$, $a = 20$ mm, $b = 30$ mm, $h = 1.5$ mm, $E = 70$ GPa, and $\theta_0 = 60°$, where $u_x = \pm 0.25$ mm, $u_y = \pm 0.25$ mm, and $2\theta_z = \pm 0.0125$ rad are the applied deformation fields.

Equivalent stiffness	Applied kinematical field	Stiffness value
k_{xx} (kN/mm)	$+u_x$ $(-u_x)$ $[-u_x$ & $u_y]$ $\{-u_x$ & $+\theta_z\}$	86.18 (41.19) [41.19] {41.19}
	$[+u_x$ & $-u_y]$ $(+u_x$ & $+\theta_z)$	[57.95] (71.90)
	$[-u_x$ & $+u_y]$ $(-u_x$ & $-\theta_z)$	[69.33] (55.34)
	$[+u_x$ & $+u_y]$ $(+u_x$ & $-\theta_z)$	[86.21] (86.37)
k_{xy} (kN/mm)	$+u_y(-u_y)$ $[-u_x$ & $-u_y]$ $\{+\theta_z$ & $-u_y\}$	48.39 (20.25) [20.25] {20.25}
	$[+u_x$ & $-u_y]$ $(-\theta_z$ & $-u_y)$	[48.46] (34.40)
	$[-u_x$ & $+u_y]$ $(+\theta_z$ & $+u_y)$	[20.25] (34.28)
	$[+u_x$ & $+u_y]$ $(-\theta_z$ & $+u_y)$	[48.44] (48.50)
k_{yx} (kN/mm)	$+u_x$ $(-u_x)$ $[-u_x$ & $-u_y]$ $\{-u_x$ & $+\theta_z\}$	48.58 (20.25) [20.25] {20.25}
	$[+u_x$ & $-u_y]$ $(+u_x$ & $+\theta_z)$	[30.55] (39.46)
	$[-u_x$ & $+u_y]$ $(-u_x$ & $-\theta_z)$	[38.61] (29.48)
	$[+u_x$ & $+u_y]$ $(+u_x$ & $-\theta_z)$	[48.40] (48.58)

Table A.2
Values of the chiral, nonreciprocal elastic moduli of a chiral metamaterial with $\alpha_0 = 30°$, $a = 20$ mm, $b = 30$ mm, $\theta_0 = 60°$, and $E = 70$ GPa when it is used through various deformation cycles.

Deformation cycle	Cycle parameters	Chiral, Nonreciprocal elastic moduli					
		$\hat{B}$	$\hat{A}$	$\hat{C}$	λ_1	λ_2	β
Dilation→Spin/Rotation	$\gamma_1 = -0.0125, \gamma_2 = -0.0125$	1716	1431	1188	1174	−733.0	587.2
	$\gamma_1 = -0.0125, \gamma_2 = 0.0125$	1716	843.7	432.4	0	0	0
	$\gamma_1 = 0.0125, \gamma_2 = 0.0125$	3592	1434	432.4	−1178	840.4	−591.9
	$\gamma_1 = 0.0125, \gamma_2 = -0.0125$	3592	2022	1188	$\cong 0$	$\cong 0$	$\cong 0$

To understand how the elastic moduli are calculated, let us consider the dilation–rotation cycle (Fig. 5), where in the first two steps, dilation $\gamma_1 = -0.0125$ and rotation $\gamma_2 = -0.0125$ are consecutively applied, and then reversed in steps 3 and 4. For this deformation cycle, the elastic moduli are calculated, as follows:

$$\begin{aligned}
\hat{B} &= (5/4b)(k_{xx}|_{\gamma_1=-0.0125,\gamma_2=0}) = 1716 \text{ MPa}\\
\hat{C} &= (5/4b)(k_{yy}|_{\gamma_1=0,\gamma_2=-0.0125}) = 1188 \text{ MPa}\\
\hat{A} &= (5/8b)(k_{xy}|_{\gamma_1=0,\gamma_2=-0.0125} + k_{yx}|_{\gamma_1=-0.0125,\gamma_2=0}) = 1431 \text{ MPa}\\
\beta &= (5/8b)(k_{xy}|_{\gamma_1=0,\gamma_2=-0.0125} - k_{yx}|_{\gamma_1=-0.0125,\gamma_2=0}) = 587.2 \text{ MPa}\\
\lambda_1 &= (5/4b)(k_{xx}|_{\gamma_1=-0.0125,\gamma_2=-0.0125} - k_{xx}|_{\gamma_1=-0.0125,\gamma_2=0}) = 1174 \text{ MPa}\\
\lambda_2 &= (5/4b)(k_{yy}|_{\gamma_1=-0.0125,\gamma_2=-0.0125} - k_{yy}|_{\gamma_1=0,\gamma_2=-0.0125}) = -733.0 \text{ MPa}
\end{aligned} \tag{A.7}$$

Appendix B. Mechanical work calculations

The chiral metamaterial can develop mechanical work when it undergoes quasistatic deformation cycles that involve deforming it with two or more coupled deformation fields. The mechanical work developed by deforming the chiral metamaterial through a closed deformation cycle can be analytically calculated by determining the cumulative work as the deformation fields change during the cycle (Eqs. (34) and (35)). According to Eqs. (34) and (35), the mechanical work developed by deforming the chiral metamaterial through the different deformation cycles shown in Fig. 5 can be determined analytically, as follows:

$$W = \int_0^{\gamma_1}(\delta w|_{\gamma_2=0}) + \int_0^{\gamma_2}(\delta w) + \int_{\gamma_1}^{0}(\delta w) + \int_{\gamma_2}^{0}(\delta w|_{\gamma_1=0}) \tag{B.1}$$

with δw as defined in Eq. (33). By calculating the integration, while observing that the moduli λ_1 and λ_2 are considered only during processes $2 \to 3$ and $3 \to 4$, the mechanical work W for these deformation cycles can be obtained in the form:

$$W = \tfrac{1}{4}\lambda_2\gamma_2^2 - \tfrac{1}{4}\lambda_1\gamma_1^2 + \beta\gamma_1\gamma_2 \tag{B.2}$$

The mechanical work developed by deforming the chiral metamaterial can also be verified based on the chiral, nonreciprocal elastic constitutive law (Eq. (29)). Consider a chiral metamaterial through a closed cycle of a sequence of dilation γ_1 and rotation γ_2 (see Fig. 5), such that in Process $1 \to 2$, the chiral metamaterial is deformed by γ_1, which is followed by deforming the metamaterial by γ_2 in Process $2 \to 3$. These two deformations are then reversed in Processes $3 \to 4$ and $4 \to 1$. First, the variations of the non-zero

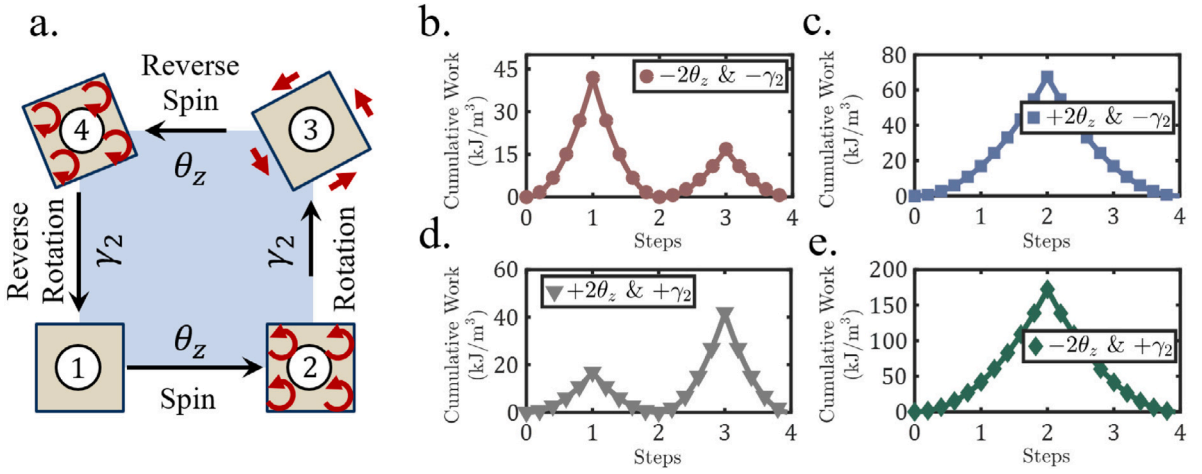

Fig. B.8. The chiral metamaterial is mechanically passive when used in spin-rotation cycles. (a) Representation of the spin-rotation cycle. (b-e) The numerical and analytical computations of the cumulative work per unit volume of the chiral metamaterial when it undergoes a sequence of quasistatic spin $2\theta_z = \pm 0.0125$ and rotation $\gamma_2 = u_{x,y} - u_{y,x} = \pm 0.0125$. The variations of the cumulative work per unit volume as the chiral metamaterial is deformed through the cycle were determined using ABAQUS finite element simulations (solid curves) and analytically based on Eq. (29) (marks). The results are represented when the chiral metamaterial was used through the same deformation sequence, while spatially inverting the spin and the rotation. Through these deformations cycles, the chiral metamaterial is reciprocal, and thus it does not develop mechanical work.

stresses σ_α through the deformation cycle are calculated based on Eq. (29), as follows:

$$\begin{aligned}
&\text{After Process } 1 \to 2 \ (\gamma_1 \text{ is applied}):\\
&\sigma_1 = \hat{B}\gamma_1 \ \& \ \sigma_2 = -\left(\hat{A} - \beta\right)\gamma_1\\
&\text{After Process } 2 \to 3 \ (\gamma_2 \text{ is applied}):\\
&\sigma_1 = \left(\hat{B} + \lambda_1\right)\gamma_1 - \left(\hat{A} + \beta\right)\gamma_2 \ \& \ \sigma_2 = -\left(\hat{A} - \beta\right)\gamma_1 + \left(\hat{C} + \lambda_2\right)\gamma_2\\
&\text{After Process } 3 \to 4 \ (\gamma_1 \text{ is reversed}):\\
&\sigma_1 = -\left(\hat{A} + \beta\right)\gamma_2 \ \& \ \sigma_2 = \hat{C}\gamma_2\\
&\text{After Process } 4 \to 1 \ (\gamma_2 \text{ is reversed}):\\
&\sigma_1 = 0 \ \& \ \sigma_2 = 0
\end{aligned} \tag{B.3}$$

Second, the work done on (or by) the chiral metamaterial during each of the four deformation processes is calculated by the area under the stress σ_i-deformation γ_i curve, i.e., $\int \delta w = \frac{1}{2}\int \left(\sigma_i \delta\gamma_i\right)$, as follows:

$$\begin{aligned}
&\text{After Process } 1 \to 2 \ (\gamma_1 \text{ is applied}):\\
&w_1 = \tfrac{1}{2}\int_0^{\gamma_1} \sigma_1|_{\gamma_2=0}\delta\gamma_1 = \tfrac{1}{4}\hat{B}\gamma_1^2\\
&\text{After Process } 2 \to 3 \ (\gamma_2 \text{ is applied}):\\
&w_2 = \tfrac{1}{2}\int_0^{\gamma_2} \sigma_2\delta\gamma_2 = -\tfrac{1}{2}\left(\hat{A} - \beta\right)\gamma_1\gamma_2 + \tfrac{1}{4}\left(\hat{C} + \lambda_2\right)\gamma_2^2\\
&\text{After Process } 3 \to 4 \ (\gamma_1 \text{ is reversed}):\\
&w_3 = \tfrac{1}{2}\int_{\gamma_1}^{0} \sigma_1\delta\gamma_1 = -\tfrac{1}{4}\left(\hat{B} + \lambda_1\right)\gamma_1^2 + \tfrac{1}{2}\left(\hat{A} + \beta\right)\gamma_2\gamma_1\\
&\text{After Process } 4 \to 1 \ (\gamma_2 \text{ is reversed}):\\
&w_4 = \tfrac{1}{2}\int_{\gamma_2}^{0} \sigma_2|_{\gamma_1=0}\delta\gamma_2 = -\tfrac{1}{4}\hat{C}\gamma_2^2
\end{aligned} \tag{B.4}$$

Finally, the mechanical work W is the value of the work accumulation over the deformation cycle, which can be calculated as the sum of the work values after the different deformation processes, as follows:

$$W = \textstyle\sum_{i=1}^{4} w_i = \tfrac{1}{4}\lambda_2\gamma_2^2 - \tfrac{1}{4}\lambda_1\gamma_1^2 + \beta\gamma_1\gamma_2 \tag{B.5}$$

It follows from Eq. (B.5) that, whereas the mechanical work W is non-zero when the chiral metamaterial is used in a closed cycle of the coupled dilation γ_1 and rotation γ_2, there is a specific combination of the dilation and rotation at which this mechanical work is zero, and this can be determined from Eq. (B.5) by $\gamma_1/\gamma_2 = (2\beta \pm \sqrt{4\beta^2 + \lambda_1\lambda_2})/\lambda_1$.

It should be noted that, because the coupling between rotation $u_{x,y} - u_{y,x}$ and spin θ_z of the chiral metamaterial is symmetric (see Fig. 4), the chiral metamaterial develops no mechanical work when used in a closed cycle of a sequence of rotation and spin deformations. We verified this analytically based on Eqs. (34) and (35) and numerically using finite element simulations, as the mechanical work for the spin-rotation cycle is always zero, as shown in Fig. B.8.

References

Asadchy, V.S., Mirmoosa, M.S., Diaz-Rubio, A., Fan, S., Tretyakov, S.A., 2020. Tutorial on electromagnetic nonreciprocity and its origins. Proc. IEEE 108 (10), 1684–1727.

Avron, J., 1998. Odd viscosity. J. Stat. Phys. 92, 543–557.

Banerjee, D., Souslov, A., Abanov, A., Vitelli, V., 2017. Odd viscosity in chiral active fluids. Nature Commun. 8, 1573.

Bowick, M.J., Fakhri, N., Marchetti, M.C., Ramaswamy, S., 2022. Symmetry, thermodynamics, and topology in active matter. Phys. Rev. X 12, 010501.

Brandenbourger, M., Locsin, X., Lerner, E., Coulais, C., 2019. Non-reciprocal robotic metamaterials. Nature Commun. 10 (1), 1–8.

Brandenbourger, M., Scheibner, C., Veenstra, J., Vitelli, V., Coulais, C., 2022. Limit cycles turn active matter into robots. arXiv:2108.08837v2.

Chen, Y., Frenzel, T., Guenneau, S., Kadic, M., Wegener, M., 2020. Mapping acoustical activity in 3D chiral mechanical metamaterials onto micropolar continuum elasticity. J. Mech. Phys. Solids 137, 103877.

Chen, Y., Kadic, M., Wegener, M., 2021a. Chiral triclinic metamaterial crystals supporting isotropic acoustical activity and isotropic chiral phonons. Proc. R. Soc. A 477, 20200764.

Chen, Y., Li, X., Scheibner, C., Vitelli, V., Huang, G., 2021b. Realization of active metamaterials with odd micropolar elasticity. Nature Commun. 12, 5935.

Condiff, D., Dahler, J., 1964. Fluid mechanical aspects of antisymmetric stress. Phys. Fluids 7, 842–854.

Correas-Serrano, D., Gomez-Diaz, J.S., Sounas, D.L., Hadad, Y., Alvarez-Melcon, A., Alù, A., 2016. Nonreciprocal graphene devices and antennas based on spatiotemporal modulation. IEEE Antennas Wirel. Propag. Lett. 15, 1529–1533.

Coulais, C., Sounas, D., Alù, A., 2017. Static non-reciprocity in mechanical metamaterials. Nature 542, 461–464.

Das, M., Schmidt, C.F., Murrell, M., 2020. Introduction to active matter. Soft Matter 16 (31), 7185–7190.

De-Groot, S.R., Mazur, P., 1962. Non-Equilibrium Thermodynamics. North-Holland Publishing Company, Amsterdam, and Jhon Wiley and Sons, Inc., New York.

Deseigne, J., Dauchot, O., Chaté, H., 2010. Collective motion of vibrated polar disks. Phys. Rev. Lett. 105, 098001.

Estep, N.A., Sounas, D.L., Soric, J., Alù, A., 2014. Magnetic-free non-reciprocity and isolation based on parametrically modulated coupled-resonator loops. Nat. Phys. 10 (12), 923–927.

Fang, K., Yu, Z., Fan, S., 2012a. Photonic Aharonov-Bohm effect based on dynamic modulation. Phys. Rev. Lett. 108 (15), 153901.

Fang, K., Yu, Z., Fan, S., 2012b. Realizing effective magnetic field for photons by controlling the phase of dynamic modulation. Nat. Photon. 6 (11), 782–787.

Fernandez-Corbaton, I., Rockstuhl, C., Ziemke, P., Gumbsch, P., Albiez, A., Schwaiger, R., Frenzel, T., Kadic, M., Wegener, M., 2019. New twists of 3D chiral metamaterials. Adv. Mater. 31, 1807742.

Frenzel, T., Kadic, M., Wegener, M., 2017. Three-dimensional mechanical metamaterials with a twist. Science 358 (6366), 1072–1074.

Frenzel, T., Köpfler, J., Jung, E., Kadic, M., Wegener, M., 2019. Ultrasound experiments on acoustical activity in chiral mechanical metamaterials. Nature Commun. 10 (1), 1–6.

Fruchart, M., Hanai, R., Littlewood, P.B., Vitelli, V., 2021. Non-reciprocal phase transitions. Nature 592, 363–369.

Ghatak, A., Brandenbourger, M., van Wezel, J., Coulais, C., 2019. Observation of non-Hermitian topology and its bulk-edge correspondence. Proc. Natl. Acad. Sci. USA 117 (47), 29561–29568.

Gong, Z., Ashida, Y., Kawabata, K., Takasan, K., Higashikawa, S., Ueda, M., 2018. Topological phases of non-Hermitian systems. Phys. Rev. X 8 (3), 031079.

Hadad, Y., Sounas, D.L., Alù, A., 2015. Space-time gradient metasurfaces. Phys. Rev. B 92 (10), 100304.

He, B., Yang, L., Jiang, X., Xiao, M., 2018. Transmission nonreciprocity in a mutually coupled circulating structure. Phys. Rev. Lett. 120 (20), 203904.

Huang, J., Zhou, X., 2019. A time-varying mass metamaterial for non-reciprocal wave propagation. Int. J. Solids Struct. 164, 25–36.

Jin, B., Argyropoulos, C., 2019. Nonreciprocal transmission in nonlinear PT-symmetric metamaterials using epsilon-near-zero media doped with defects. Adv. Opt. Mater. 7 (23), 1–10.

Joumaa, H., Ostoja-Starzewski, M., 2011. Stress and couple-stress invariance in non-centrosymmetric micropolar planar elasticity. Proc. R. Soc. A 467 (2134), 2896–2911.

Kudrolli, A., Lumay, G., Volfson, D., Tsimring, L., 2008. Swarming and swirling in self-propelled polar granular rods. Phys. Rev. Lett. 100, 058001.

Kumar, N., Soni, H., Ramaswamy, S., Sood, A.K., 2014. Flocking at a distance in active granular matter. Nature Commun. 5, 4688.

Kunst, F.K., Dwivedi, V., 2019. Non-Hermitian systems and topology: A transfer-matrix perspective. Phys. Rev. B 99 (24), 245116.

Lakes, R., 2001. Elastic and viscoelastic behavior of chiral materials. Int. J. Mech. Sci. 43 (7), 1579–1589.

Lakes, R.S., Benedict, R.L., 1982. Noncentrosymmetry in micropolar elasticity. Internat. J. Engrg. Sci. 20 (10), 1161–1167.

Li, L., Lee, C.H., Gong, J., 2019a. Geometric characterization of non-Hermitian topological systems through the singularity ring in pseudospin vector space. Phys. Rev. B 100 (7), 075403.

Li, M., Ni, X., Weiner, M., Alù, A., Khanikaev, A.B., 2019b. Topological phases and nonreciprocal edge states in non-Hermitian Floquet insulators. Phys. Rev. B 100 (4), 045423.

Liu, X., Hu, G., 2016. Elastic metamaterials making use of chirality: A review. Strojniški Vestnik - J. Mech. Eng. 62, 403–418.

Liu, X.N., Huang, G.L., Hu, G.K., 2012. Chiral effect in plane isotropic micropolar elasticity and its application to chiral lattices. J. Mech. Phys. Solids 60, 1907–1921.

Lu, Z., Norris, A.N., 2020. Non-reciprocal wave transmission in a bilinear spring-mass system. J. Vib. Acoust. Trans. ASME 142 (2), 021006.

Mahmoud, A., Davoyan, A., Engheta, N., 2015. All-passive nonreciprocal metastructure. Nature Commun. 6, 1–7.

Markovich, T., Tjhung, E., Cates, M.E., 2019. Chiral active matter: Microscopic 'torque dipoles' have more than one hydrodynamic description. New J. Phys. 21, 112001.

Naganathan, S., Fürthauer, S., Nishikawa, M., Jülicher, F., Grill, S., 2014. Active torque generation by the actomyosin cell cortex drives left-right symmetry breaking. Elife 3, e04165.

Naganathan, S., Middelkoop, T., Fürthauer, S., Grill, S., 2016. Actomyosin-driven left-right asymmetry: From molecular torques to chiral self organization. Curr. Opin. Cell Biol. 38, 24–30.

Nash, L.M., Kleckner, D., Read, A., Vitelli, V., Turner, A.M., Irvine, W.T., 2015. Topological mechanics of gyroscopic metamaterials. Proc. Natl. Acad. Sci. USA 112, 14495–14500.

Nassar, H., Chen, Y., Huang, G., 2019. Isotropic polar solids for conformal transformation elasticity and cloaking. J. Mech. Phys. Solids 129, 229–243.

Nassar, H., Chen, Y.Y., Huang, G.L., 2020a. Polar metamaterials: A new outlook on resonance for cloaking applications. Phys. Rev. Lett. 124, 084301.

Nassar, H., Yousefzadeh, B., Fleury, R., Ruzzene, M., Alù, A., Daraio, C., Norris, A.N., Huang, G., Haberman, M.R., 2020b. Nonreciprocity in acoustic and elastic materials. Nat. Rev. Mater. 5, 667–685.

Natroshvili, D., Stratis, I.G., 2006. Mathematical problems of the theory of elasticity of chiral materials for Lipschitz domains. Math. Methods Appl. Sci. 29 (4), 445–478.

Palacci, J., Sacanna, S., Steinberg, A.P., Pine, D., Chaikin, P., 2013. Living crystals of light-activated colloidal surfers. Science 339, 936–940.

Patteson, A.E., Gopinath, A., Arratia, P.E., 2018. The propagation of active-passive interfaces in bacterial swarms. Nature Commun. 9, 5373.

Rosa, M.I., Ruzzene, M., 2020. Dynamics and topology of non-Hermitian elastic lattices with non-local feedback control interactions. New J. Phys. 22 (5), 053004.

Rubenstein, M., Cornejo, A., Nagpal, R., 2014. Programmable self-assembly in a thousand-robot swarm. Science 345, 795–799.

Sabrina, S., Spellings, M., Glotzer, S.C., Bishop, K.J.M., 2015. Coarsening dynamics of binary liquids with active rotation Soft Matter. Proc. Natl. Acad. Sci. USA 11, 8409.

Sanchez, T., Chen, D.N., DeCamp, S., Heymann, M., Dogic, Z., 2012. Spontaneous motion in hierarchically assembled active matter. Nature 491, 431–434.
Schaller, V., Weber, C., Semmrich, C., Frey, E., Bausch, A., 2010. Polar patterns of driven filaments. Nature 467, 73–77.
Scheibner, C., Souslov, A., Banerjee, D., Surówka, P., Irvine, W.T., Vitelli, V., 2020. Odd elasticity. Nat. Phys. 16 (4), 475–480.
Shaat, M., 2020. Nonreciprocal elasticity and the realization of static and dynamic nonreciprocity. Sci. Rep. 10, 21676.
Shaltout, A., Kildishev, A., Shalaev, V., 2015. Time-varying metasurfaces and Lorentz non-reciprocity. Opt. Mater. Express 5 (11), 2459–2467.
Shankar, S., Souslov, A., Bowick, M.J., Marchetti, M.C., Vitelli, V., 2020. Topological active matter. arXiv:2010.00364v2 [Cond-Mat.Soft].
Sirota, L., Ilan, R., Shokef, Y., Lahini, Y., 2020. Non-Newtonian topological mechanical metamaterials using feedback control. Phys. Rev. Lett. 125 (25), 256802.
Smith, M., 2009. ABAQUS/Standard User's Manual, Version 6.9. United States: Dassault Systémes Simulia Corp.
Soni, V., Bililign, E.S., Magkiriadou, S., Sacanna, S., Bartolo, D., Shelley, M.J., Irvine, W.T.M., 2015. The odd free surface flows of a colloidal chiral fluid. Nat. Phys. 15, 1188–1194.
Sounas, D.L., Caloz, C., Alù, A., 2013. Giant non-reciprocity at the subwavelength scale using angular momentum-biased metamaterials. Nature Commun. 4, 2407.
Sumino, Y., Nagai, K., Shitaka, Y., Tanaka, D., Yoshikawa, K., Chaté, H., Oiwa, K., 2012. Large-scale vortex lattice emerging from collectively moving microtubules. Nature 483, 448–452.
Taravati, S., Caloz, C., 2017. Mixer-duplexer-antenna leaky-wave system based on periodic space-time modulation. IEEE Trans. Antennas and Propagation 65 (2), 442–452.
Theurkauff, I., Cottin-Bizonne, C., Palacci, J., Ybert, C., Bocquet, L., 2012. Dynamic clustering in active colloidal suspensions with chemical signaling. Phys. Rev. Lett. 108, 268303.
Tjhung, E., Cates, M., Marenduzzo, D., 2017. Contractile and chiral activities codetermine the helicity of swimming droplet trajectories. Proc. Natl. Acad. Sci. USA 114, 4631–4636.
Trainiti, G., Xia, Y., Marconi, J., Cazzulani, G., Erturk, A., Ruzzene, M., 2019. Time-periodic stiffness modulation in elastic metamaterials for selective wave filtering: Theory and experiment. Phys. Rev. Lett. 122 (12), 124301.
Vasquez, F.G., Milton, G.W., Onofrei, D., Seppecher, P., 2012. In: Craster, R.V., Guenneau, S. (Eds.), Transformation Elastodynamics and Active Exterior Acoustic Cloaking in Acoustic Metamaterials: Negative Refraction, Imaging, Lensing and Cloaking. Springer, Dordrecht, pp. 289–318.
Voituriez, R., Joanny, J.-F., Prost, J., 2005. Spontaneous flow transition in active polar gels. Europhys. Lett. 70, 404.
Wu, W., Hu, W., Qian, G., Liao, H., Xu, X., Berto, F., 2019. Mechanical design and multifunctional applications of chiral mechanical metamaterials: A review. Mater. Des. 180, 107950.
Xu, X., Wang, C., Shou, W., Du, Z., Chen, Y., Li, B., Matusik, W., Hussein, N., Huang, G., 2020. Physical realization of elastic cloaking with a polar materia. Phys. Rev. Lett. 124, 14301.
Yao, S., Song, F., Wang, Z., 2018. Non-Hermitian chern bands. Phys. Rev. Lett. 121 (13), 136802.
You, Z., Baskaran, A., Marchetti, M.C., 2020. Nonreciprocity as a generic route to traveling states. Proc. Natl. Acad. Sci. USA 117, 19767–19772.
Zhang, H., Chen, Y., Liu, X., Hu, G., 2020. An asymmetric elastic metamaterial model for elastic wave cloaking. J. Mech. Phys. Solids 135, 103796.
Zhao, Y., Zhou, X., Huang, G., 2020. Non-reciprocal Rayleigh waves in elastic gyroscopic medium. J. Mech. Phys. Solids 143, 104065.